Journal of MATERIALS RESEARCH

Invited Feature Paper - Review

DOI: 10.1557/jmr.2020.27

FOCUS ISSUE

HETEROGENEITY IN 2D MATERIALS

Manufacturing strategies for wafer-scale two-dimensional transition metal dichalcogenide heterolayers

Mengjing Wang[1], Hao Li[2], Tae-Jun Ko[1], Mashiyat Sumaiya Shawkat[3], Emmanuel Okogbue[3], Changhyeon Yoo[1], Sang Sub Han[4], Md Ashraful Islam[3], Kyu Hwan Oh[5], Yeonwoong Jung[6,a)]

[1]*NanoScience Technology Center, University of Central Florida, Orlando, Florida 32826, USA*
[2]*NanoScience Technology Center, University of Central Florida, Orlando, Florida 32826, USA; and Department of Materials Science and Engineering, University of Central Florida, Orlando, Florida 32826, USA*
[3]*NanoScience Technology Center, University of Central Florida, Orlando, Florida 32826, USA; and Department of Electrical and Computer Engineering, University of Central Florida, Orlando, Florida 32816, USA*
[4]*NanoScience Technology Center, University of Central Florida, Orlando, Florida 32826, USA; and Department of Materials Science and Engineering, Seoul National University, Seoul 08826, South Korea*
[5]*Department of Materials Science and Engineering, Seoul National University, Seoul 08826, South Korea*
[6]*NanoScience Technology Center, University of Central Florida, Orlando, Florida 32826, USA; Department of Materials Science and Engineering, University of Central Florida, Orlando, Florida 32826, USA; and Department of Electrical and Computer Engineering, University of Central Florida, Orlando, Florida 32816, USA*
[a)]Address all correspondence to this author. e-mail: yeonwoong.jung@ucf.edu

This paper has been selected as an Invited Feature Paper.

Received: 21 October 2019; accepted: 13 January 2020

Modern electronics have been geared toward exploring novel electronic materials that can encompass a broad set of unusual functionalities absent in conventional platforms. In this regard, two-dimensional (2D) transition metal dichalcogenide (TMD) semiconductors are highly promising, owing to their large mechanical resilience coupled with superior transport properties and van der Waals (vdW) attraction-enabled relaxed assembly. Moreover, 2D TMD heterolayers based on chemically distinct constituent layers exhibit even more intriguing properties beyond their mono-component counterparts, which can materialize only when they are manufactured on a technologically practical wafer-scale. This mini-review provides a comprehensive overview of recent progress in exploring wafer-scale 2D TMD heterolayers of various kinds. It extensively surveys a variety of manufacturing strategies and discusses their scientific working principles, resulting 2D TMD heterolayers, their material properties, and device applications. Moreover, it offers extended discussion on remaining challenges and future outlooks toward further improving the material quality of 2D TMD heterolayers in both material and manufacturing aspects.

Introduction

The development of low-dimensional nanomaterials (e.g., carbon nanotubes, one-dimensional (1D) nanowires, and two-dimensional (2D) layered materials) presents tremendous opportunities in the enrichment of life quality by bringing forth previously conceptually projected devices and technologies into reality [1, 2, 3]. Following the discovery of graphene, a monolayer of graphite, 2D layered materials have been gaining significant attention because of a large set of their unusual yet superior material properties enabled by coupling of extremely small physical dimension and van der Waals (vdW)-assisted anisotropic crystallinity [4, 5, 6]. These intrinsically unique features have prompted the expansion of 2D material libraries covering a broad spectrum of band structures from insulating to semiconducting and metallic [6, 7, 8, 9, 10], e.g., hexagonal boron nitride (*h*-BN), black phosphorus (BP), silicene, transition metal dichalcogenides (TMDs), and transition metal carbides/nitrides (MXenes). Among these 2D material series, TMDs have received extensive attention because of their superior optical and electrical attributes, such as visible-wavelength band gap with intrinsic tunability, high carrier mobility, and high on/off current ratio [11, 12, 13, 14, 15, 16], many of which are unattainable in graphene [6, 17]. With the provision of these advantages, 2D TMDs have found extensive applications in a wide range of novel electronics and optoelectronics devices, e.g., near atom thickness circuitry, extremely low-power transistors, and tunable band gap energy accompanying its indirect-to-direct transition, which were foreseen to be challenging to realize otherwise [6, 9, 10, 18, 19, 20]. In addition to their electrical and optical merits, 2D TMDs also possess exceptional mechanical properties with high elasticity and flexibility, owing to their extremely small vertical thickness and large in-plane strain limits, allowing them to be applicable to mechanically reconfigurable devices such as flexible transistors, wearable sensors, and foldable displays [7, 8, 17].

Beyond these intrinsic property advantages inherent to single-component 2D TMDs, heterogeneously integrating multiple 2D TMD layers of controlled composition and morphology is envisioned to bring out even more exotic properties [21, 22]. Unlike the covalently bonded 3D compound thin films, the assembly of 2D TMD layers with distinct components is facilitated by weak vdW attraction across individually isolated 2D layers. This structural uniqueness can lead to a variety of 2D TMD "heterolayers" based on vertically stacked multiple 2D layers of distinct compositions, which can overcome major technical limitations with traditional thin-film growths. Conventional approaches to prepare for heterostructured 3D compound thin films suffer from the "lattice match constraint," i.e., only certain materials possessing similar crystalline structure and lattice parameters to those of their underlying components can be heterogeneously assembled to maintain good crystalline quality with the minimal mismatch [23]. These combined advantages of extraordinary material properties and relaxed assembly requirements inherent to 2D TMDs enable unprecedented opportunities as verified in extensive proof-of-concept demonstrations employing 2D TMD heterolayers. For instance, the band structures of 2D TMD heterolayers can be precisely tuned via appropriate band alignment and interlayer coupling, which encourages the design of highly efficient electronics or optoelectronic devices such as band gap–optimized solar cells, *p*–*n* diodes, and field-effect transistors (FETs) [14, 15, 24, 25, 26, 27, 28, 29, 30]. Moreover, vertically integrating 2D TMD layers of judiciously selected components can realize an entirely new form of atomically thin materials whose properties can be further modulated by subtle structural variations such as crystallographic misorientations [31, 32, 33, 34, 35].

Despite these foreseen grand opportunities, fabrications of 2D TMD heterolayers with controlled chemistry and morphology have been technically challenging, resulting in the limitation of their projected device applications. The technical difficulty becomes particularly pronounced in terms of scaling them up to a technologically more relevant "wafer-scale," so 2D TMD heterolayers can be more compatible with already established thin-film semiconductor manufacturing schemes. Indeed, current methods for the preparation of 2D TMD heterolayers have relied on the manual stacking of individual 2D TMD flakes, which is not intrinsically scalable, thus remains impractical. Ideal manufacturing strategies should encompass atomic-level morphological precision and wafer-level spatial scalability, yielding 2D TMD heterolayers with a large lateral dimension allowing for subsequent fabrication processes and a small vertical dimension ensuring the intrinsic structural uniqueness of atomically thin materials. Moreover, incorporation of unwanted structural and chemical defects (e.g., bubbles, wrinkles, and contaminants) should be minimized, resulting in atomically-sharp and seamless 2D/2D hetero-interfaces.

This mini-review overviews recent progress in manufacturing strategies for "wafer-scale" 2D TMDs-based vertically stacked heterolayers. We comprehensively survey a variety of versatile approaches capable of fabricating such materials, including chemical vapor deposition (CVD)-based direct growth and sequential integration of pre-CVD grown and transferred 2D layers [30, 36, 37]. We introduce their working principles and highlight the unique material properties of 2D TMD heterojunctions maintained on the wafer-scale and explore their present applications in electronics and optoelectronics. We also verify challenging issues with the current status of wafer-scale 2D TMD heterolayers, including technical limitations of their manufacturing strategies as well as drawbacks in their material properties. Last, we discuss the prospects of these emerging materials and propose forward-looking suggestions for overcoming their remaining issues toward paving the way for further advancement and eventual commercialization. Figure 1 provides an illustrational overview of the subjects covered in this review.

Manufacturing strategies

A substantial amount of research effort has recently been devoted to fabricating wafer-scale 2D TMD heterolayers by employing chemical and physical methods. As the foundation of such endeavors, recently developed property-preserving strategies for their growth, transfer, and integration will be discussed in detail in the following section.

Direct growth of wafer-scale 2D TMD heterolayers

Metal film transformation

Earlier approaches based on chemical growth or mechanical exfoliation of individual 2D layers have been limited to yielding 2D TMD heterolayers of very small sizes, so they are not scalable, patternable, and practical. Metal thin film transformation refers to the approach that fabricates wafer-scale

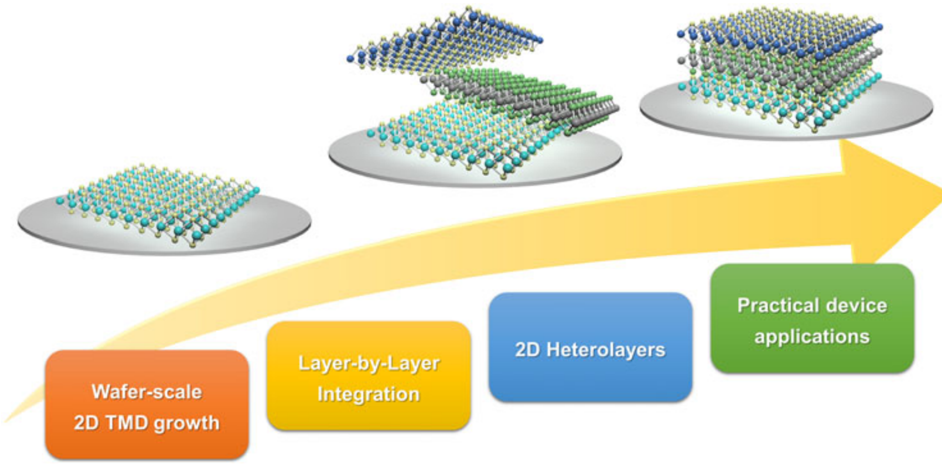

Figure 1: Schematics of the topics covered in this review. (color online)

homogeneous 2D TMD layers by chemically reacting predeposited metal thin films (e.g., Mo, W, and Pt) with vaporized chalcogen reagents (e.g., S, Se, and Te) [38, 39, 40]. The structural morphology and crystallographic orientation of 2D TMD layers can be tuned by modulating the thickness of starting metal films; e.g., horizontally or vertically aligned 2D layers are grown by thin or thick metal films, respectively [38, 40]. In this approach, the lateral dimension of grown 2D TMD layers is precisely determined by that of starting metal films, which offers suitability for fabricating wafer-scale 2D TMD heterostructures. This fabrication is carried out in either "one-step" transforming predeposited entire metal films or "two-step" sequentially growing distinct 2D TMD layers with one on top of the other. Details are discussed as follows.

A one-step metal film transformation method was explored as alternatives to yield 2D TMD heterolayers sharing identical chalcogen elements, e.g., MoS_2/WS_2 and $MoSe_2/WSe_2$. A schematic of the growth process is shown in Fig. 2(a). Elemental metal films of Mo and W with controlled thickness are sequentially deposited on SiO_2/Si growth substrates using a metal shadow mask via magnetron sputtering or e-beam evaporation. The metal-stacked substrates are then subsequently reacted with vaporized chalcogen elements [e.g., sulfur (S) or selenium (Se)] in a low-pressure CVD chamber, which yields vertical-stacks of 2D TMD heterolayers. Figure 2(b) shows an image of wafer-scale vertically stacked MoS_2/WS_2 heterolayers [36] and Fig. 2(c) demonstrates the patternability of this one-step metal film transformation method achieving patterned MoS_2/WS_2 heterolayers [37]. Figure 2(d) exhibits Raman spectroscopy profiles evidencing a presence of both MoS_2 and WS_2 in the heterolayers, contrast to the characteristics obtained from mono-component 2D TMDs [37]. Figure 2(e) shows a plane-view TEM image of vertically stacked MoS_2/WS_2 heterolayers revealing their polycrystalline nature, as evidenced in the electron diffraction pattern in the inset. Figure 2(f) shows a high-angle annular dark-field (HAADF) cross-sectional scanning TEM (STEM) image of the heterolayers, revealing their well-resolved layer morphology and sharp image contrast in between each region [41]. Figure 2(g) shows energy dispersive X-Ray spectroscopy (EDS) map images of Mo and W corresponding to Fig. 2(f), evidencing their spatially well-defined distribution. This one-step metal film transformation method can be applied to fabricate "laterally" patterned wafer-scale 2D TMD heterolayers as well, as demonstrated in Fig. 2(h) [42]. Figure 2(i) shows EDS elemental map images of Mo and W localized laterally-patterned MoS_2/WS_2 heterolayers. Figure 2(j) presents a plane-view high-resolution (HRTEM) image obtained from an interface of MoS_2/WS_2, revealing that both materials are grown in a vertically aligned orientation in this case.

In addition to the above-discussed one-step growth method, the two-step growth of wafer-scale 2D TMD heterolayers has been explored via a sequential metal film transformation process that mimics the sequential stacking of individual 2D layers in chemical or physical manners [22, 43]. Wu et al. demonstrated large-area growth of 2D MoS_2/WS_2 heterostructures of uniform layer number (i.e., five MoS_2 layers and four WS_2 layers) on a sapphire substrate by combining sequential sulfurization and metal deposition [44]. As shown in Fig. 2(k), the first layer of metal seeds (Mo: 1 nm thickness) was deposited on the sapphire substrate via an RF sputter and was placed inside the central zone of a tube furnace. At the upstream of the tube furnace, a preloaded sulfur powder was thermally evaporated and reacted with the Mo-sapphire substrate at 800 °C, achieving the first stack of 2D layers (i.e., five MoS_2 layers). Subsequently, the second layer of metal seeds (W: 1 nm thickness) was deposited on the pregrown 2D MoS_2 layers and underwent the identical transformation process as the first stack, achieving four WS_2 layers on top of the. Characteristic Raman peaks of these wafer-scale

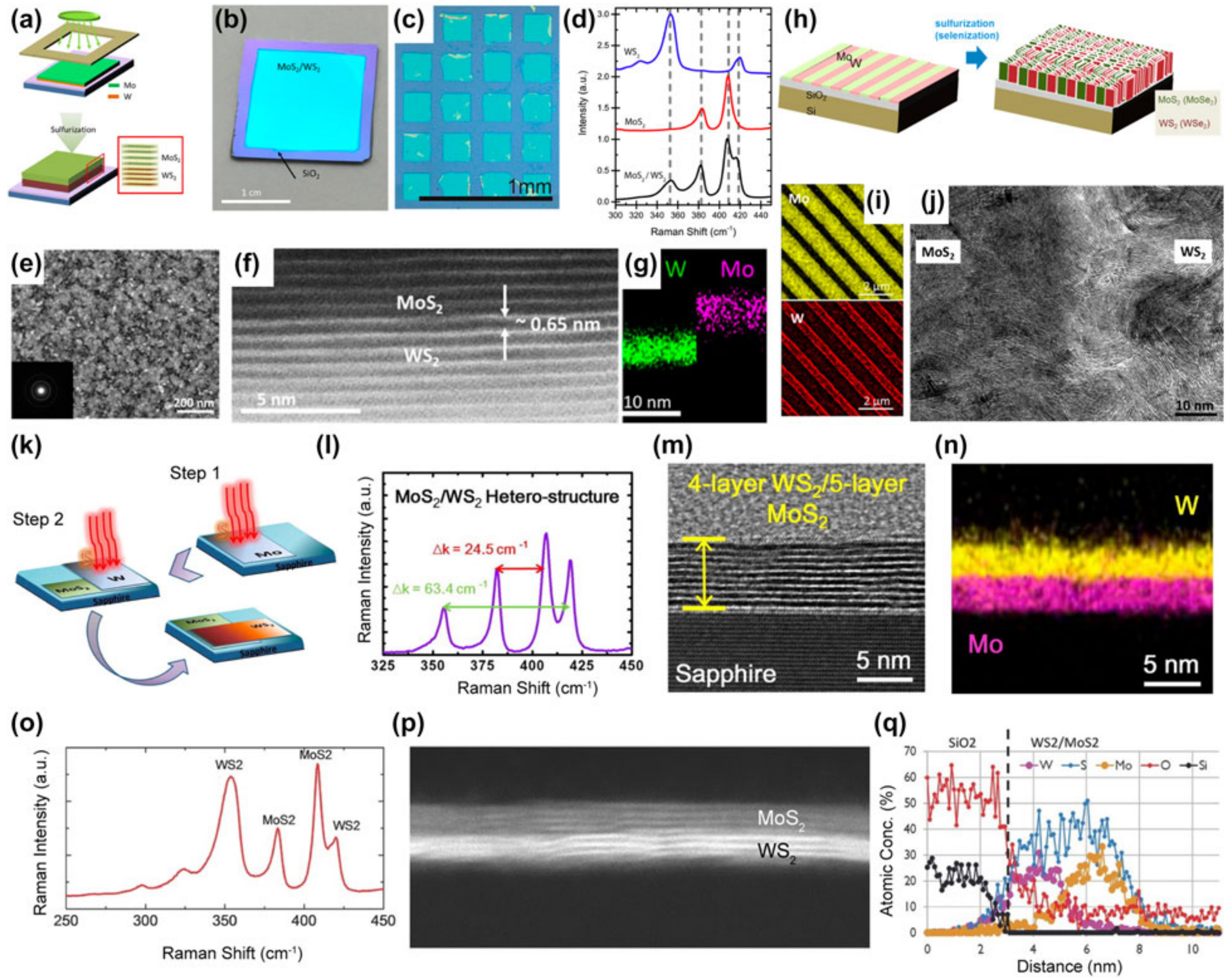

Figure 2: (a–j) One-step metal film transformation growth of 2D TMD heterolayers. (a) Schematic process for the growth of vertically stacked MoS_2/WS_2 heterolayers. (b) Wafer-scale MoS_2/WS_2 heterolayers. (c) Patterned array of MoS_2/WS_2 heterolayers. (d) Raman spectra of individual MoS_2 and WS_2 as well as MoS_2/WS_2 heterolayers. (e) In-plane HRTEM image of vertically stacked MoS_2/WS_2 heterolayers. (f) Cross-sectional TEM of vertically stacked MoS_2/WS_2 heterolayers. (g) EDS elemental map images corresponding to (f). (h) Schematic process for the metal film transformation growth of laterally patterned MoS_2/WS_2 heterolayers. (i) EDS elemental images showing the localized distribution of Mo and W corresponding to the schematic in (h). (j) Plane-view HRTEM image obtained at an interface of MoS_2/WS_2 corresponding to (i). (k–q) Two-step sequential metal film transformation growth of 2D TMDs heterolayers achieved with two different precursors for vaporized sulfur. (k–n) Thermal evaporation of sulfur powder. (o–q) Direct flow of H_2S. (k) The schematics of the two-step metal film transformation growth procedure based on a sequential thermal sulfurization of Mo and W seeds. (l) Raman spectroscopy. (m) Cross-sectional HRTEM, and (n) HAADF element mapping characterization of MoS_2/WS_2 heterolayers obtained by the sequential thermal sulfurization method. (o) Raman spectroscopy. (p) Cross-sectional HRTEM, and (q) EDS line scan characterization of WS_2/MoS_2 heterolayers obtained by thermal annealing of sequentially deposited W and Mo seeds under H_2S gas flow. (a, b) Reprinted with permission from Ref. [36]. Copyright 2016 Nature Publishing Group. (c, d) Reprinted with permission from Ref. [37]. Copyright © 2016, American Chemical Society. (e–g) Reprinted with permission from Ref. [41]. Copyright © 2017, American Chemical Society. (h–j) Reprinted with permission from Ref. [42]. Copyright © 2014, American Chemical Society. (k–n) Reprinted with permission from Ref. [44]. Copyright © 2016, American Chemical Society. (o–q) Reprinted with permission from Ref. [43]. Copyright © 2015, Wiley-VCH Verlag GmbH & Co. KGaA, Weinheim. (color online)

2D MoS_2/WS_2 layers are presented in Fig. 2(l), indicating the presence of both targeted components. For the identification of their crystal quality, cross-sectional HRTEM and STEM-EDS characterizations were conducted. Figure 2(m) shows an HRTEM cross-sectional view of 2D TMD heterostructures composed of a well-resolved total of nine layers. Figure 2(n) presents its corresponding HAADF STEM elemental mapping image, visualizing a localized elemental distribution of Mo and W, identifying the existence of five MoS_2 and four WS_2 layers. Moreover, this TEM analysis clarifies that this sequential metal film transformation process can yield atomically sharp and seamless 2D/2D hetero-interfaces. Chiappe et al. have reported a similar two-step sequential metal film transformation method using hydrogen sulfide (H_2S) gas as a precursor instead of the thermal evaporation of sulfur powder [43]. This vaporized precursor was claimed to offer better control of the uniformity of metal film transformation process, achieving 2D TMD layers of higher material quality [43]. For the two-step sequential growth, an initial layer of W was deposited on a SiO_2/Si wafer and was subsequently sulfurized under H_2S gas at 800 °C in a lamp-based annealing system. After that, the second layer of Mo was deposited on the pregrown 2D WS_2 layers and was reacted under H_2S gas for the growth of 2D MoS_2 layers. The formation of 2D WS_2/MoS_2 heterolayers was confirmed by Raman spectroscopy and cross-sectional TEM analysis. Figure 2(o) reveals four distinguishable Raman characteristic peaks denoting the A_{1g} and E_{2g} vibration modes of MoS_2 and WS_2 layers. The dark-field cross-sectional TEM image in Fig. 2(p) reveals obvious image contrast between MoS_2 and WS_2 as well as their well-resolved 2D layer morphology. Figure 2(q) shows an EDS line scan spectrum across the 2D/2D hetero-interfaces in Fig. 2(p), further evidencing a localized distribution of constituting elements without significant intermixing.

Although this metal film transformation method has been successfully applied to fabricate wafer-scale 2D TMD polycrystalline heterostructures, some key challenges and issues remain to be resolved. For instance, the resulting wafer-scale 2D TMD heterostructures generally contain a large concentration of structural defects (e.g., grain boundaries) which lead to that their electrical properties (e.g., carrier mobility) often do not reach the level demanded in high-performance electronics. This limitation results from that the deposited metal films provide enormous heterogeneous nucleation sites contributed by a large number of constituent metal nanoparticles, which is inevitable because of their deposition nature. These excessive heterogeneous nucleation sites suppress the continued growth of 2D layer crystals, resulting in a large number of grain boundaries with small-sized individually crystalline grains. This challenge at present remains unsolved, requiring the in-depth investigation of 2D TMD nucleation and growth mechanism at the atomistic level.

Vapor phase deposition

In addition to the metal film transformation approach, vapor phase deposition methods that grow 2D TMD crystals through the crystallization of molecular reactants released from gas phased precursors have been widely employed for fabricating large-area 2D TMDs heterostructures. Examples of these approaches include powder vapor transport (PVT) or powder source CVD [45, 46, 47], metal–organic CVD (MOCVD) [48, 49, 50], and molecular beam epitaxy (MBE) [51, 52, 53]. In contrast to the metal film transformation, these vapor phase deposition techniques offer common advantages of more precisely controlling the thickness of individual 2D layer grains down to the monolayer-level as well as achieving higher single crystallinity within each grain. 2D TMD heterostructures fabricated by these vapor phase deposition methods usually follow two distinct epitaxial growth modes, i.e., out-of-plane vertical or in-plane edge-driven epitaxial expansion. Examples of 2D heterostructures fabrication through above vapor phase deposition approaches will be discussed in detail below.

PVT or powder source CVD process was initially explored and can grow crystalline 2D TMD layer domains with small layer numbers [45, 47]. Gong et al. reported the growth of single-crystalline 2D WS_2/MoS_2 heterostructures by using this powder source CVD method and achieved the lateral dimension of ~20 μm for each crystalline grain [30]. Solid powders containing W, molybdenum trioxide (MoO_3), and tellurium were simultaneously evaporated in the flow of sulfur vapor to supply their corresponding vaporized reactants, and the distinct nucleation and growth rates of each 2D TMD led to the sequential growth of heterostructures rather than alloying. However, its intrinsic limitation with precisely controlling the vapor pressure of reactants converted from their solid powders poses severe limitations toward wafer-scale fabrication of 2D TMD heterostructures. Accordingly, the 2D WS_2/MoS_2 heterostructures were sparsely grown on the substrates without entirely covering them, exhibiting a significant spatial inhomogeneity. MOCVD is an alternative growth technique which supplies vapor-phased volatile metal–organic precursors with modulated flux concentration. As it can control the stacking and thickness of 2D TMD layers by controlled pulse sequences, in principle, it is more suitable for the large-area growth of 2D TMD heterostructures with improved spatial homogeneity than the PVT method [48, 49, 50]. Lin et al. demonstrated the sequential epitaxial growth of 2D vertical MoS_2/WSe_2 heterostructures on graphene by combining MOCVD with oxide powder vaporization [54]. As shown in Fig. 3(a), 2D WSe_2 layers were synthesized by reacting metal–organic $W(CO)_6$ and $(CH4)_2Se$ precursors at 800–850 °C on three-layer graphene. Subsequently, 2D MoS_2 layers were grown on top of the pregrown 2D WSe_2 layers at 750 °C by the PVT method using MoO_3 and sulfur powders. The Raman spectrum in Fig. 3(b) and corresponding cross-sectional STEM images in Figs. 3(c) and 3(d) confirm the material quality and the stacking sequence of resulting 2D TMD heterostructures. The sharp and clean interfaces from the cross-sectional STEM images further verify that there is no alloying between the first and the second 2D TMD layers during the growth. However, the lateral dimension of the individual crystalline domains of 2D TMD heterostructures obtained by this MOCVD method remains to be approximately a few square micrometers at present, indicating that much efforts are needed toward their growth parameter optimization.

MBE relies on the molecular reaction of high purity metal sources under ultrahigh vacuum conditions and has been utilized for the growth of ultrathin, highly crystalline 2D TMD layers such as 2D $MoSe_2$ [55] and 2D WSe_2 [56]. Recently, Dai et al. grew 2D $WSe_2/MoSe_2$ heterostructures using a customized MBE reactor equipped with reflection high-energy electron diffraction (RHEED) which monitors the whole growth process [57]. 2D WSe_2 layers were first grown

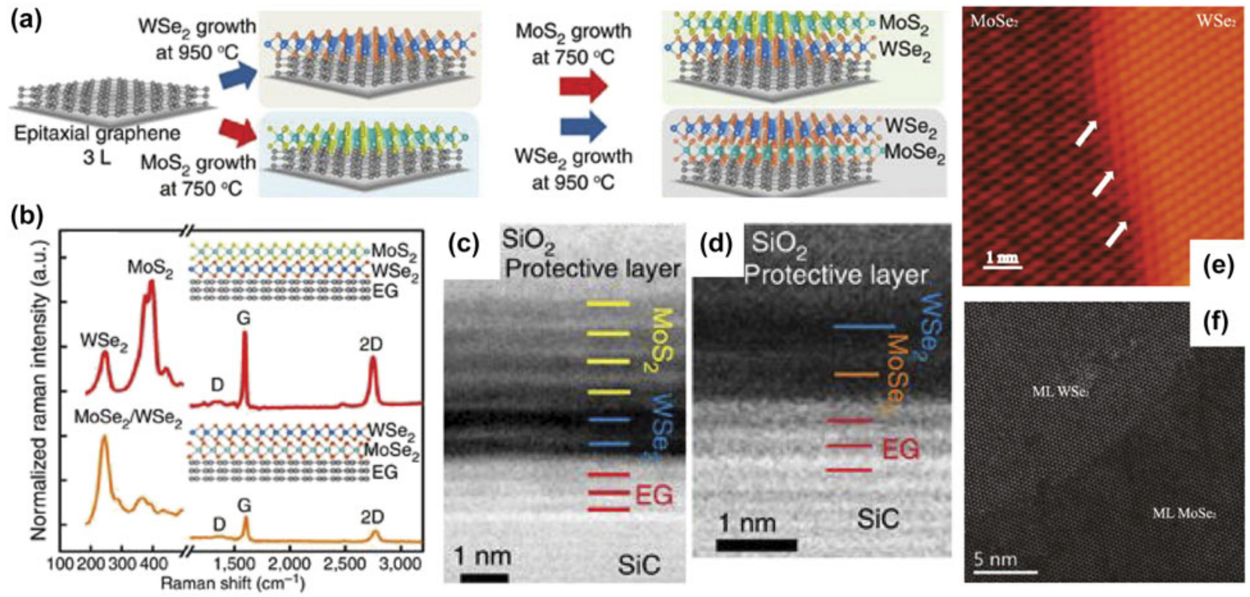

Figure 3: (a–d) Fabrication of 2D TMD heterostructures through combined MOCVD and oxide vapor vaporization. (a) Schematic illustration for the sequential growth of 2D TMD layers on top of graphene. (b) Raman spectra obtained from 2D WSe_2/MoS_2 and 2D MoS_2/WSe_2 heterostructures grown on graphene, and (c, d) corresponding cross-sectional STEM images of the hetero-interfaces in each material. (e) STM image and (f) ADF-STEM image of laterally stitched 2D $MoSe_2/WSe_2$ heterostructures grown by MBE. (a–d) Reprinted with permission from Ref. [54]. Copyright © 2015, Springer Nature. (e, f) Reprinted with permission from Ref. [57]. Copyright © 2019, American Chemical Society. (color online)

in the MBE reactor by mixing the flux of W and Se elements at a constant temperature of 500–550 °C followed by an additional annealing process which removes residual W. Subsequently, 2D $MoSe_2$ layers were grown by supplying the flux of Mo element only, which resulted in 2D $WSe_2/MoSe_2$ lateral heterojunctions. The atomic-resolution scanning tunneling microscopy (STM) image in Fig. 3(e) and the ADF-STEM image in Fig. 3(f) reveal the atomically sharp, lateral interface of 2D $WSe_2/MoSe_2$ heterolayers, evidencing their in-plane stitching growth.

Although all these vapor phase deposition methods are generally desirable for achieving high crystallinity and small thickness of individual 2D layer grains, it is noteworthy that resulting 2D heterostructures suffer from several issues at present, e.g., incomplete coverage of the entire growth wafer because of unevenly grown 2D layers, a spatial inhomogeneity of chemical compositions over a large scale, as well as complications in preparing for vapor-phased precursors and precisely optimizing their material parameters (e.g., vapor pressure). Accordingly, wafer-scale 2D TMD heterolayers with their targeted material quality have not been produced yet.

Transfer- and integration-based fabrication of wafer-scale 2D TMD heterolayers

Although some of the above-discussed direct synthetic approaches have successfully demonstrated the growth of wafer-scale 2D TMD heterolayers, several technical challenges remain unresolved. Examples of characteristic limitations include difficulties in achieving uniform layer number and spatial homogeneity avoiding chemical variations at 2D/2D interfaces over an entire wafer-scale, as well as complications in controlling the stacking order/orientation of distinct 2D layer components limited by high-temperature growth conditions. Solutions to resolve these issues have been pursued by exploring viable "post-growth" approaches that can individually transfer pregrown 2D layers of distinct chemical components from initial growth substrates and integrate them into secondary target substrates in a scalable and controllable manner. In this section, we will overview up-to-date progress in achieving 2D TMD heterostructures by post-growth transfer/integration methods in detail. Some representative approaches include thermal release tape (TRT) enabled programmed vacuum stack (PVS), mechanical crack enabled transfer/integration, water-assisted transfer/integration, and polymers assisted transfer/integration.

TRT enabled PVS

Kang et al. adopted the MOCVD technique and succeeded in depositing a variety of wafer-scale 2D TMD monolayers (i.e., MoS_2, $MoSe_2$, and WS_2) [58]. Then, they employed a TRT to as-grown 2D layers of various components and subsequently detached/integrated them under vacuum utilizing a custom-built layer stacking system, termed a PVS method. In this method, a TRT/adhesive film is conformally attached to the first layer (L0) and then peeled off from the growth substrate.

Subsequently, the TRT/adhesive film with L0 is pressed onto the next layers (L1, L2, ...) by making intimate contact between L0 and them under vacuum, and this stacking step can be repeated until targeted stacking sequences are completed. Lastly, a heating step is carried out to weaken the adhesion between the TRT/adhesive film and L0, resulting in the integration of 2D TMD heterostructures (L0/L1/L2/...) onto receiver substrates [59]. Figure 4 presents the wafer-scale manufacturing of various 2D heterolayers achieved by the application of TRT-enabled PVS method [58]. Figure 4(a) depicts the schematic of vertically stacked wafer-scale 2D heterolayers composed of nine alternating monolayers of MoS_2 and WS_2 to be realized by the TRT-enabled PVS method. Figure 4(b) demonstrates a cross-sectional STEM image verifying the experimental realization of these targeted 2D heterolayers, revealing spatially uniform composition and atomically abrupt interfaces formed by adjacent individual 2D layers. The annular dark field (ADF)-STEM image in Fig. 4(b), left portrays five layers of MoS_2 and four layers of WS_2 with alternating dark and bright contrast, respectively. Furthermore, the interlayer spacing between MoS_2 and WS_2 is observed to be 6.4 Å, which is in agreement with the previously reported interlayer spacing of MoS_2/WS_2 with a nonzero rotation angle [60]. The electron energy loss spectroscopy (EELS) characterization in Fig. 4(b) right reveals the localization of Mo peaks within the MoS_2 layers as well as a low concentration of impurity carbon, indicating the high material quality of the achieved 2D heterolayers. Figure 4(c) exhibits Raman frequency map images of E_{2g}^{1} frequency over a 40 μm × 40 μm area of one-, two- (top), and five (bottom) 2D MoS_2 layers, revealing their spatial homogeneity. Figure 4(d) schematically elucidates the TRT-enabled PVS process steps for the wafer-scale fabrication of 2D TMD heterolayers. It is noted that this PVS method seems to be viable if the adhesion of monolayer-to-TRT film is stronger than that of monolayer-to-growth-substrate. The success of 2D layers integration is also strongly dependent on the environmental conditions (e.g., humidity) under which individual layers are stacked as well as their intrinsic surface states. Since this PVS method avoided the involvement of chemical etchants or solvents for stacking 2D layers, this method was able to achieve 2D/2D hetero-interfaces of superior quality compared with other approaches, which can be evidenced by combinational characterization of the optical image, atomic force microscopy (AFM), XRD, and cross-sectional TEM. Figure 4(e) shows the optical image of wafer-scale 2D MoS_2 layers (L0) on TRT after initial peeling (left) as well as two additional MoS_2 layers (L1 and L2) after final integration (right). Figure 4(f) compares the AFM topography of 2D MoS_2 layers whose transfer and integration was carried out in vacuum (left) and air (right). The results highlight the clean surface of the samples prepared by the vacuum-based PVS method, unlike those prepared in the air which contain a large degree of surface defects [61, 62, 63]. The material quality of the wafer-scale 2D MoS_2 layers integrated by the PVS method was further characterized by X-ray diffraction (XRD). Figure 4(g) compares the XRD peak intensities of the samples prepared by the vacuum-based PVS method versus by the conventional mechanical-exfoliation, indicating fiver times higher intensity for the former approach attributed to the clean interface of prepared 2D layers (inset). Given their intrinsic vdW bonding nature, it has been projected that individual 2D layers can be assembled in a layer-by-layer manner avoiding the lattice-match constraint prevailing in thin-film epitaxial growths [21, 22]. Figure 4(h) presents the cross-sectional STEM image of vertically stacked heterolayers based on three different 2D TMDs, i.e., $MoSe_2/MoS_2/WS_2$, directly evidencing the projected vdW-enabled assembly despite their large lattice mismatch and interlayer rotation.

Mechanical cracking-enabled transfer and integration

Another transfer-based technique that has been developed for the wafer-scale integration of 2D TMDs is the layer-resolved splitting (LRS) method [64, 65]. Compared to other previously developed methods mainly adopted for the transfer of small-sized 2D layer flakes [22, 66, 67], this LRS method reported by Shim et al. allows for the wafer-scale isolation of individual 2D monolayers from a variety of as-grown thick 2D TMDs in a chemical-free manner. Individually isolated 2D monolayers can be subsequently stacked up, achieving wafer-scale 2D heterolayers [23, 65, 68]. This process is based on the interfacial toughness (Γ) difference of as-grown 2D layers versus growth substrates, employing nickel (Ni) film as an atomic-scale adhesive. Figure 5(a) shows the schematic depiction of the LRS transfer process. Following the growth of initially thick 2D TMD layers on a growth substrate (e.g., sapphire), Ni adhesive film is deposited on top of the as-grown material, and the entire stack of wafer-scale Ni/2D TMD layers is subsequently detached from the original substrate. This separation step is possible because the Γ between Ni and 2D TMD layers (Γ_{2D-Ni}) [69] is greater than that of the vdW interfaced individual 2D TMD layers (Γ_{2D-2D}) [70] which is in turn greater than the Γ between the 2D TMD layers and the substrate ($\Gamma_{2D-Sapphire}$), i.e., $\Gamma_{2D-Ni} > \Gamma_{2D-2D} > \Gamma_{2D-Sapphire}$. Once the entire stack of 2D TMD multilayers is removed from the sapphire wafer, the LRS process is repeated until the continuous 2D TMD layers on the bottom can be split into many monolayers which become transferred to secondary host substrates. Figure 5(b) illustrates the schematics of crack progression during LRS for the initial exfoliation of entire 2D TMD stacks from the growth substrate (left) and the exfoliation of the bottom monolayer 2D TMD

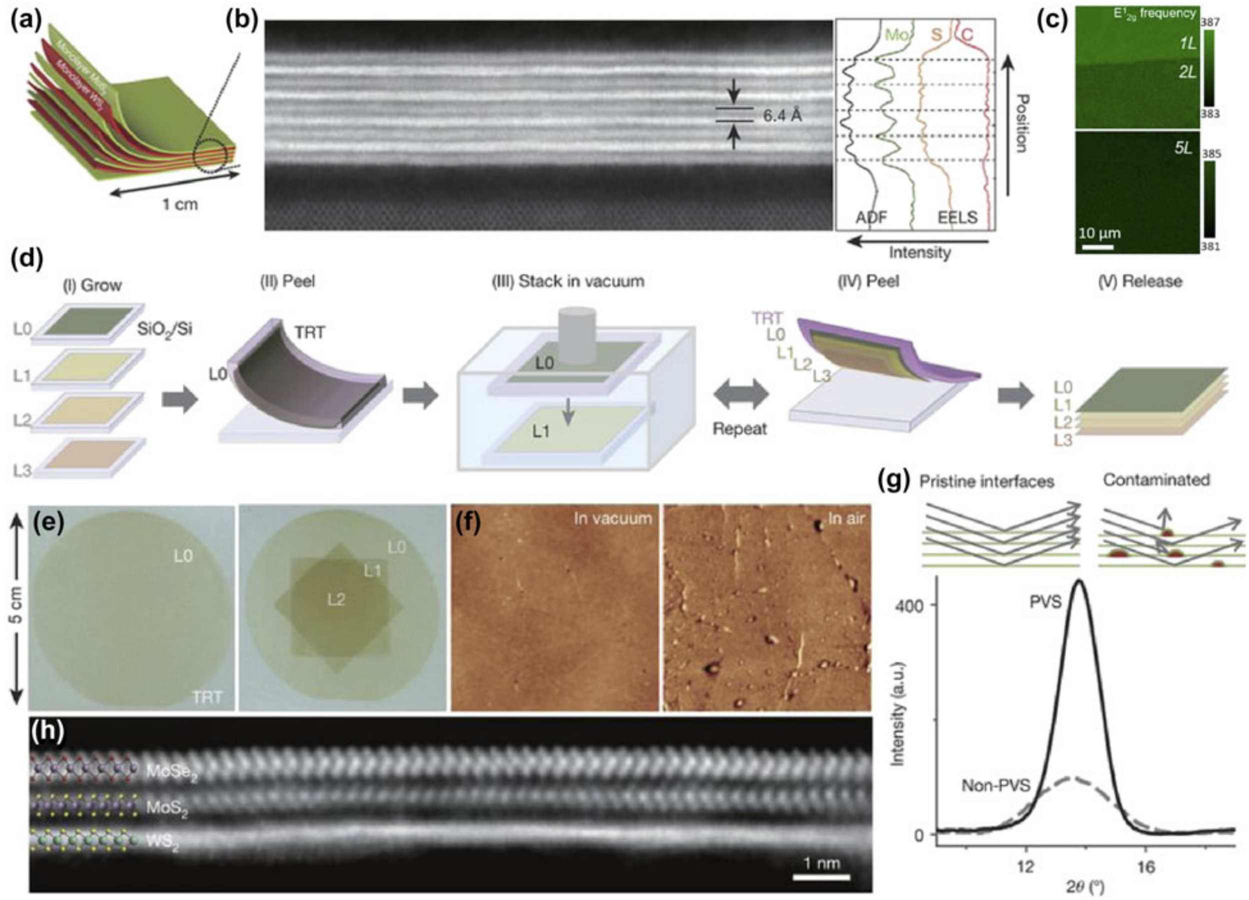

Figure 4: Layer-by-layer assembly of 2D TMDs into wafer-scale heterostructures by the PVS method. (a) Schematic of vertically assembled nine alternating monolayers of MoS_2 and WS_2. (b) Cross-sectional ADF STEM image of 2D heterolayers (left) and their EELS characterization (right) corresponding to (a). (c) Raman frequency mapping of E_{2g}^{1} peak across one and two layers (top) as well as five layers of 2D MoS_2 (bottom). (d) A schematic of the PVS process. (e) Optical images of 2D MoS_2 monolayer at the initial state (L0; left) and after the integration of two more layers (L1 and L2) on L0 (right). (f) AFM topography images of the L2 side of the three 2D MoS_2 layers assembled in a vacuum (left) and air (right). (g) XRD peaks obtained from four 2D MoS_2 layers assembled by the PVS (solid curve) versus non-PVS (dashed curve) method. (h) Cross-sectional STEM image of vertically stacked $MoSe_2/MoS_2/WS_2$ heterolayers (a–h) Reprinted with permission from Ref. [58]. Copyright © 2017, Springer Nature. (color online)

(right) based on the interfacial toughness correlation of constituting components. The external force applied when lifting the adhesive Ni deposited top layer results in torque across the sample which initiates a fracture, leading to that the crack propagates downward [64, 71]. Application of a bending moment during the lift-off of a Ni/2D TMD stack supplies elastic strain energy to the bottom interfaces. Figure 5(c) presents modeling results that show that the strain energy per unit area is released on 2D TMD layers delamination once reaching the desired strain release rate, further justifying the working principle. This method has been utilized in the fabrication of wafer-scale heterostructures of *h*-BN, MoS_2, and WS_2 with uniform properties across the wafer [64].

Water-assisted transfer and integration

In addition to the abovementioned "dry" transfer method, Kim et al. developed a water-based "wet" transfer method which can transfer and integrate wafer-scale 2D TMD layers of various components onto virtually arbitrary substrates [72]. The main advantage of this water-assisted method is in that it utilizes water only avoiding any other chemical etchants or polymeric protective materials previously developed for 2D layers delamination processes which may decorate their material properties [73, 74, 75]. Accordingly, it ensures chemically benign and structurally clean transfer and integration of various 2D TMD layers, greatly broadening their versatility for realizing wafer-scale 2D TMD heterolayers. Figure 6(a) illustrates the schematic procedure of the water-assisted transfer and integration of 2D TMD layers. First, metal (e.g., Mo) seed layers are deposited on a SiO_2/Si wafer with a hydrophilic surface wettability. Subsequently, the metal-deposited wafer undergoes the previously established CVD thermal reaction [20, 38, 72, 76, 77, 78, 79, 80, 81] which converts the metal to desired 2D TMD layers (e.g., Mo to 2D MoS_2 layers). Then, the prepared sample is immersed in water, which causes the spontaneous

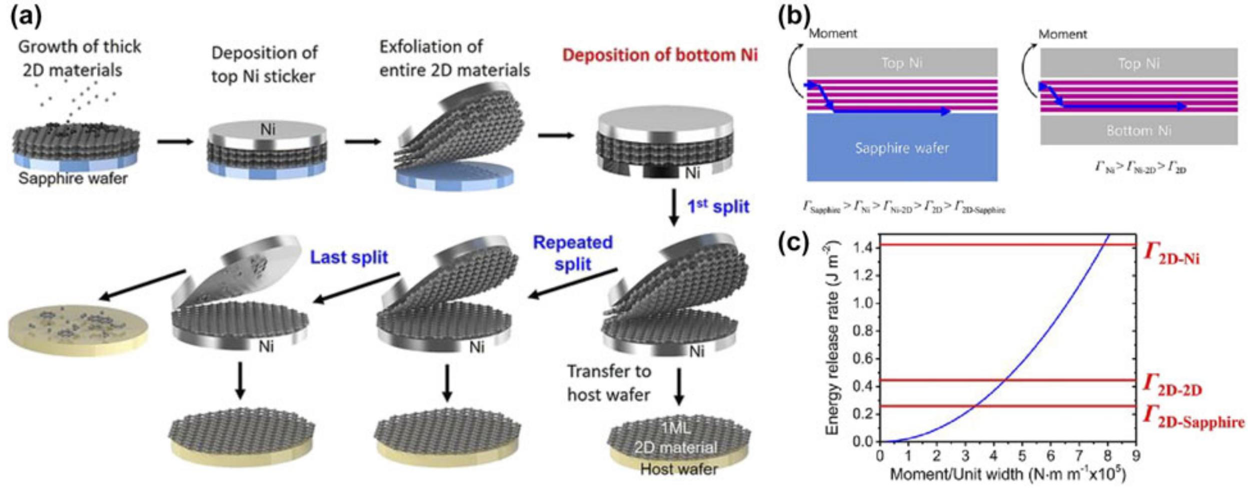

Figure 5: Mechanical cracking-enabled transfer and integration of wafer-scale 2D TMD heterolayers. (a) Schematic description of the LRS process for 2D TMD layers transfer and integration. (b) Schematic depiction of the crack progression for initial exfoliation of thick multilayer 2D TMDs from their growth substrate (left) and exfoliation of the bottom monolayer 2D TMD (right). (c) Modeling of the energy release rate according to the applied moment exerted at various interfaces of 2D-Ni, 2D-2D, and 2D-sapphire. (a–c) Reprinted with permission from Ref. [64]. Copyright © 2018, American Association for the Advancement of Science. (color online)

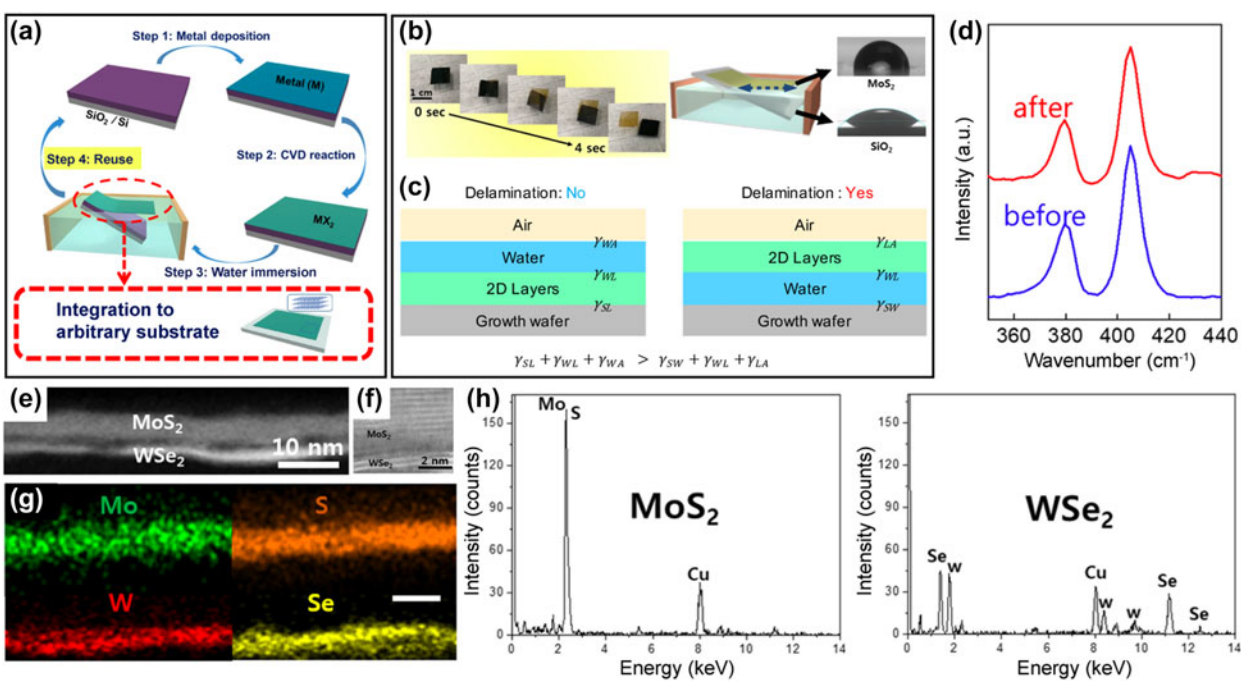

Figure 6: Water-assisted transfer and integration of wafer-scale 2D TMD heterolayers. (a) Schematic illustration of the transfer and integration procedure. (b) Time-lapsed images of water-assisted delamination of 2D MoS_2 layers (left) and their corresponding schematic to illustrate its working principle (right). (c) Thermodynamic consideration of energy requirement for water-assisted delamination of 2D layers. (d) Raman characterization of 2D MoS_2 layers before and after their transfer and integration. (e) A cross-sectional TEM image of vertically stacked MoS_2/WSe_2 heterolayers and (f) its corresponding interfacial morphology. (g) Elemental map images showing the spatial distribution of Mo, W, S, and Se. The scale bar is 10 nm. (h) EDS spectra obtained from MoS_2 (left) and WSe_2 (right) in (g). (a, b, d–h) Reprinted with permission from Ref. [72]. Copyright © 2019, Springer Nature. (color online)

delamination of 2D layers floating on the water surface, retaining their original shape and size. The delaminated 2D layers are manually integrated onto secondary substrates inside water, and the remaining SiO_2/Si wafer can be repeatedly reused for the subsequent growth of other 2D TMDs layers. Accordingly, it is possible to grow and integrate a series of distinct 2D layers from a single wafer in an unlimited manner, offering a significant advantage of material and process sustainability. The success in this water-assisted 2D layer delamination is attributed to the surface energy imbalance in between 2D TMD layers versus SiO_2/Si. Figure 6(b) shows an experimental demonstration of the water-assisted delamination of wafer-scale 2D MoS_2 layers (left) and describes its underlying principle (right). The surface of SiO_2/Si wafers in their pristine form intrinsically exhibits high hydrophilicity because of the disordered nature of amorphous SiO_2 [82]. This surface hydrophilicity can be drastically pronounced to be "superhydrophilicity" on controlled irradiation of Ar or O_2 plasma which further promotes the structural disorder and/or introduces OH^- functional groups [76, 83, 84]. Accordingly, this highly hydrophilic SiO_2 surface presents very large surface energy, whereas high-quality 2D TMD layers intrinsically exhibit high hydrophobicity with small surface energy, owing to their defects-mediated sp^2 covalent bonded basal planes [85]. These distinct surface states are confirmed by the significant difference in the contact angles of liquid droplets deposited on each surface, as demonstrated in Fig. 6(b), right. The validity of this working principle is further analyzed by the following thermodynamic consideration based on the interfacial energy difference of each component participating in the 2D layer delamination event. Figure 6(c) illustrates the two different configurations of 2D TMD layers/growth wafers, highlighting the requirement for thermodynamic conditions; (i) The summation of interfacial energies for when 2D layers become delaminated (right) should be smaller than that for when 2D layers do not get delaminated (left); i.e., $\gamma_{SL} + \gamma_{WL} + \gamma_{WA} > \gamma_{SW} + \gamma_{WL} + \gamma_{LA}$, where W, A, L, S represents water, air, 2D layers, and growth wafer, respectively. (ii) The penetration of water in between the 2D layers and the underlying growth wafers should be exerted by a sufficient amount of driving force, i.e., work of adhesion, $W_{ad} = \gamma_{SW} + \gamma_{WL} - \gamma_{SL} > 0$. By considering these two conditions, we can conclude that $0 < W_{ad} < \gamma_{WL} + \gamma_{WA} - \gamma_{LA}$, which indicates that the 2D layers/air interfacial energy (γ_{LA}), i.e., the surface energy of 2D layers, should be minimized to ensure a large enough driving force to facilitate water penetration. Given that this method involves water only for processing 2D TMD layers, they perfectly preserve their initial structural and chemical integrity throughout the delamination, transfer, and integration procedures. Figure 6(d) compares the Raman characterization spectra of 2D MoS_2 layers before and after their transfer and integration, which reveals nearly identical characteristics [72]. These combined advantages of facile transfer and integration processes, as well as the preservation of materials properties, have been utilized to assemble vertically stacked wafer-scale 2D TMD layers of distinct components. Figure 6(e) shows a cross-sectional TEM image of 2D TMD heterolayers fabricated by vertically assembling 2D MoS_2 layers on top of preprepared 2D WSe_2 layers, exhibiting sharp imaging contrast from each region. Figure 6(f) shows their corresponding interfacial morphology, revealing the well-preserved morphology of individual 2D layers. Figure 6(g) presents the corresponding ADF-STEM elemental map images, revealing that individual constituting elements are well localized in the targeted locations throughout the vertically stacked layers. Figure 6(h) shows the corresponding EDS spectra obtained from the MoS_2 (left) and WSe_2 (right) regions, evidencing their stoichiometric existence. The previously explored one-step or two-step metal film transformation growth methods (discussed in Fig. 2) are limited to achieve 2D TMD heterolayers sharing identical chalcogen atoms in each layer (e.g., S in MoS_2/WS_2 [30, 43, 86, 87] and Se in $MoSe_2/WSe_2$ [54, 88, 89]) due to the thermal degradation of materials which happens when dissimilar chalcogen atoms are reacted during CVD growths [90, 91]. As this water-assisted method is intrinsically not limited by the chemical composition of 2D TMD layers, it can achieve 2D TMD heterolayers of arbitrary stacking orders offering improved versatility.

Polymer-assisted transfer and integration

Previous works on the transfer and integration of mechanically exfoliated or chemically grown individual 2D flakes have mainly employed polymeric adhesives to lift them off from their growth substrates. Some of these approaches include methyl/n-butyl methacrylate copolymer (Elvacite® 2550 acrylic resin) [92], poly(dimethylsiloxane) (PDMS) [93, 94, 95, 96], PDMS and water-assisted hybrid (wedging transfer method) [97], as well as poly(methylmethacrylate) (PMMA) [98, 99, 100, 101, 102, 103, 104, 105]. The PMMA-assisted transfer and integration method is one of the most extensively explored approaches and has been adopted for fabricating various 2D vdW heterostructures [98, 99, 100, 101, 102, 103, 104, 105]. However, it still presents a variety of adverse attributes such as the introduction of residual impurities because of the incomplete removal of PMMA and mechanical damage of 2D layers because of its nonconformal contact between them and target substrates [106, 107], as well as limited transferability toward hydrophobic 2D layer surfaces [98, 108]. Accordingly, wafer-scale fabrication of vertically stacked 2D TMD heterolayers has remained as a nontrivial issue. Boandoh et al. developed a modified polymer-assisted transfer and integration method to fabricate wafer-scale 2D TMD heterolayers employing a freestanding viscoelastic polymer support layer (VEPSL) [108]. Figure 7 illustrates the schematic procedure of the VEPSL-enabled 2D layer transfer and integration. Dissolved polyethylene (PE) in cyclohexanone is spin-coated onto the topmost 2D TMD layer followed by curing at 90 °C which is above its glass transition temperature. A stack of TMD/VEPSL layer is spontaneously detached from its growth substrate, and it was attached to separately prepared additional 2D TMD layers for the integration of 2D

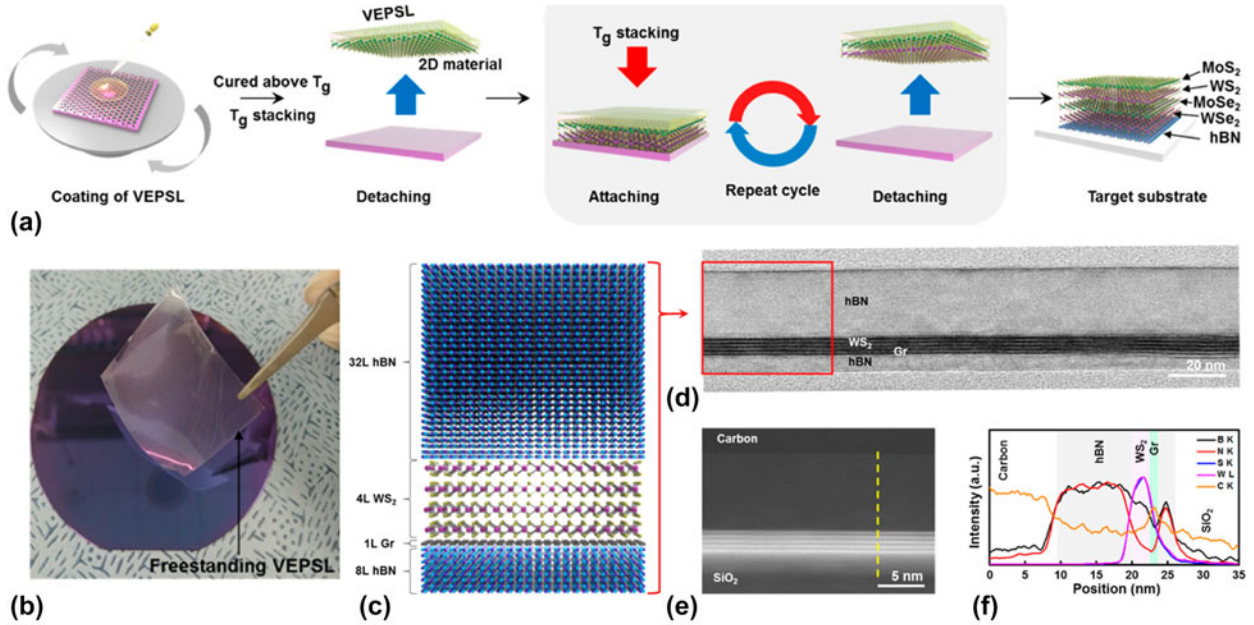

Figure 7: Polymer-assisted transfer and integration of 2D TMD heterolayers using the VEPSL method. (a) Schematic illustration of layer-by-layer stacking of 2D layers with freestanding VEPSL. (b) Image of freestanding VEPSL for large-scale assembly of diverse 2D layers. (c) Schematics of VEPSL-assembled *h*-BN/WS_2/Graphene/*h*-BN heterolayers (d) Cross-sectional ABF-STEM image. (e) Corresponding ADF-STEM image of the selected area in (d). (f) STEM-EDS line profile along the yellow dashed line in (e). (a–f) Reprinted with permission from Ref. [108]. Copyright © 2019, American Chemical Society. (color online)

heterolayers [108]. This cycle of 2D layer detachment and attachment is repeated until desired materials are achieved. The construction of random-sequence 2D vdW heterostructures (e.g., MoS_2/WS_2/$MoSe_2$/WSe_2/*h*-BN) is projected to be possible through their manual stacking via the aid of a freestanding VEPLS. Figure 7(b) shows an image of freestanding VEPSL attached 2D layer detached from its growth substrate. Figures 7(c)–7(e) demonstrate the fabrication of complex vertically stacked 2D TMD-based heterostructures of well-defined layer numbers, i.e., *h*-BN (32 layers)/WS_2 (4 layers)/graphene (1 layer)/*h*-BN (8 layers) as shown in Fig. 7(c). Figures 7(d) and 7(e) show representative cross-sectional TEM images of the assembled vdW heterostructure, i.e., annular bright-field (ABF) and ADF STEM images, respectively. The structure of four-layer WS_2 and one-layer graphene sandwiched between multilayer *h*-BN films (top and bottom layers) is clearly visible. Because only the topmost *h*-BN layer came in contact with the VEPSL, all the interfaces in the vdW heterostructure remain clean over the whole region [108]. Figure 7(f) shows the EDS spectrum obtained across the yellow dotted line in Fig. 7(e), further supporting the successful construction of the targeted vdW heterostructure. Compared with the conventional employed PMMA method [98, 99], this freestanding VEPLS method is claimed to achieve an easier and more conformal transfer of 2D layers to the substrates of any geometry including rough, groove, and terrace-like surfaces [108].

Properties and applications of wafer-scale 2D TMD heterolayers

The above-discussed wafer-scale strategies for the growth, transfer, and integration of 2D TMDs heterolayers have paved the way for exploring unusual yet exciting properties and applications on them at a technologically relevant length scale. The following subsections will discuss recent research progress toward such endeavors.

Shim et al. employed the above-introduced LRS method to fabricate wafer-scale 2D *h*-BN/WS_2/*h*-BN heterolayers and explored their optoelectronic and electrical properties for device applications [64]. Figure 8(a) shows the transfer curves of gate voltage versus drain current, evidencing the encapsulation of *h*-BN over WS_2 significantly reduces hysteresis as it efficiently suppresses deleterious trap charges from the substrate [109, 110, 111]. Wu et al. also fabricated FETs employing wafer-scale 2D TMD heterolayers by the sequential two-step metal film transformation growth of 2D MoS_2 and 2D WS_2 layers introduced in the previous section [44]. Figure 8(b) compares their performances to standalone 2D MoS_2-based devices showing a significant increase in their drain current. Opto-electrical properties of the MoS_2/WS_2 heterolayers achieved by the sequential metal transformation method were also evaluated via ultraviolet photoelectron spectroscopy (UPS) together with absorption measurements, and compared to those of standalone MoS_2 and WS_2 layers. Figure 8(c) shows

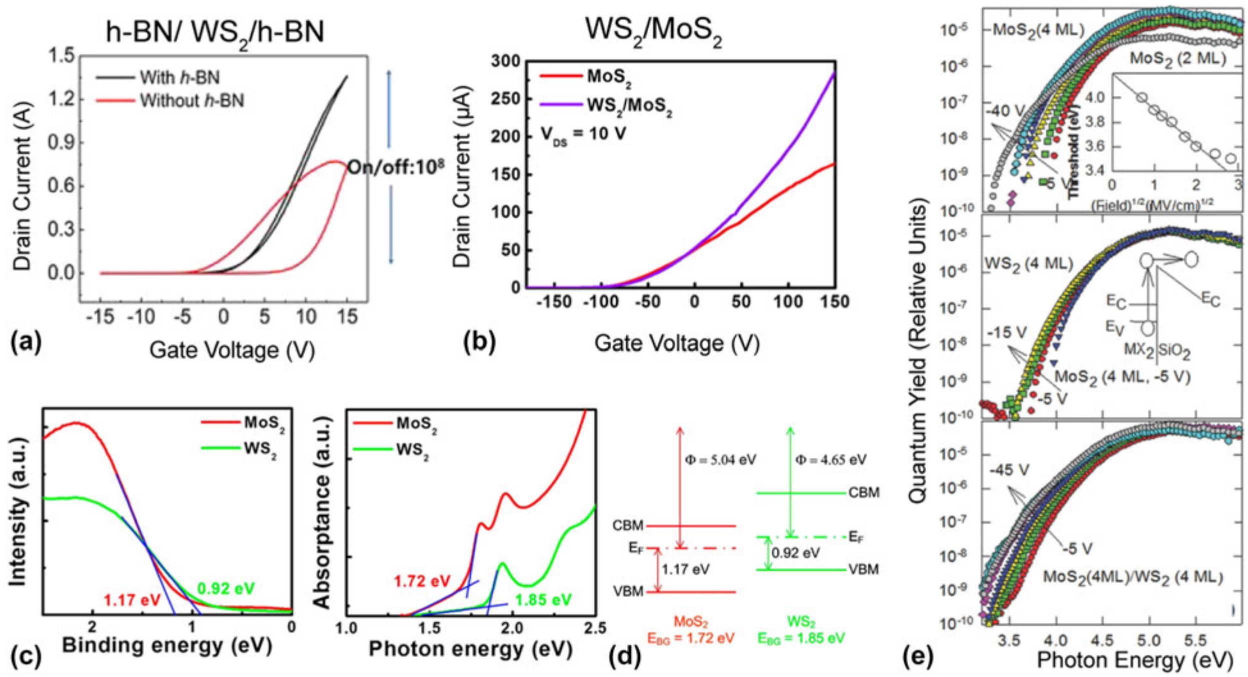

Figure 8: Properties and applications of wafer-scale 2D TMD heterolayer-based devices. (a) FET performance comparison of the LRS-enabled wafer-scale 2D MoS_2 layers with (*h*-BN/WS_2/*h*-BN heterolayers) and without *h*-BN. (b) FET transfer characteristics of standalone MoS_2 and WSe_2/MoS_2 heterolayers. (c) UPS spectra of standalone MoS_2 and WS_2 layers in low-binding energy tail (left) and their corresponding absorption spectra (right). (d) Band alignment of MoS_2/WS_2 heterolayers determined by the UPS measurements in (c). (e) Spectral plots of IPE quantum yield measurements on various 2D TMD standalone and heterolayers. (a) Reprinted with permission from Ref. [64]. Copyright © 2018, American Association for the Advancement of Science. (b–d) Reprinted with permission from Ref. [44]. Copyright © 2016, American Chemical Society. (e) Reprinted with permission from Ref. [43]. Copyright © 2015, Wiley-VCH Verlag GmbH & Co. KGaA, Weinheim. (color online)

UPS characteristics of standalone MoS_2 and WS_2 in low—(left) binding energy tail, and their corresponding absorption spectra (right), determining their work function and bandgap energy values. With these experimentally obtained parameters, the Type II band alignment of MoS_2/WS_2 heterolayers is depicted in Fig. 8(d), which is in agreement with theoretical predictions [44]. Moreover, Chiappe et al. explored the band alignment of wafer-scale MoS_2/WS_2 heterolayers obtained by the similar executed sequential metal film transformation method [43]. Figure 8(e) shows the internal photoemission (IPE) spectral of MoS_2 (top), WS_2 (mid) and WS_2/MoS_2 heterolayers (bottom), determining their quantum yields. It is observed that the valence bands of the MoS_2 and WS_2 are nearly aligned owing to the similarity between their spectral thresholds. Besides, the quantum yield obtained from the heterolayers shows little difference as compared to those obtained from the standalone 2D layers, suggesting that the sulfides possess the same valence band top energy, also affirming the common anion rule for sulfides of metals [43, 112].

Wafer-scale 2D TMD heterolayers based on vertically stacked distinct 2D layers (e.g., MoS_2/WS_2) have also presented interesting electrical properties for emerging device applications. Kang et al. fabricated wafer-scale tunneling devices employing an array of vertically stacked MoS_2/WS_2 patterns sandwiched between Au electrodes, as shown in Fig. 9(a) [58]. Figure 9(b) illustrates three different tunneling devices based on MoS_2-only, WS_2-only, and MoS_2/WS_2, all of which are in a cross-bar geometry possessing identical 2D layer numbers; i.e., six layers for both MoS_2- and WS_2-only and three/three layers for MoS_2/WS_2. The inset schematics in the bottom column present the zero-bias band diagrams corresponding to each device. Figure 9(c) elucidates the tunneling band diagram obtained with Au electrodes with these devices, indicating an efficient transport of electrons through the vdW gaps within constituting 2D layers. Figure 9(d) shows the current density (J)–voltage (V) characteristics of 2D MoS_2 layers sandwiched within top/bottom Au electrodes with varying layer numbers (denoted by N_L). The results show a significant increase of tunneling resistance with increasing layer number (e.g., $>10^4$ with the layer number change from three to seven), as anticipated from the band diagrams in Fig. 9(b). Figure 9(e) shows J–V curves measured from MoS_2, WS_2, and WS_2/MoS_2 devices with identical layer number (i.e., $N_L = 6$.) in a low bias range of -0.02 V to 0.02 V. Figure 9(f) exhibits J–V curves obtained from WS_2/MoS_2 heterolayers in a larger bias range of -1.5 V to 1.5 V, specifying characteristics under reverse bias ($V < 0$), zero-bias ($V \approx 0$) and forward bias ($V > 0$) as well as their corresponding barrier-height offset diagrams. The results show that the device presents diode-like asymmetric J–V characteristics, which is attributed to the enhanced electron

Journal of Materials Research ■ Volume 35 ■ Issue 11 ■ Jun15, 2020 ■ www.mrs.org/jmr

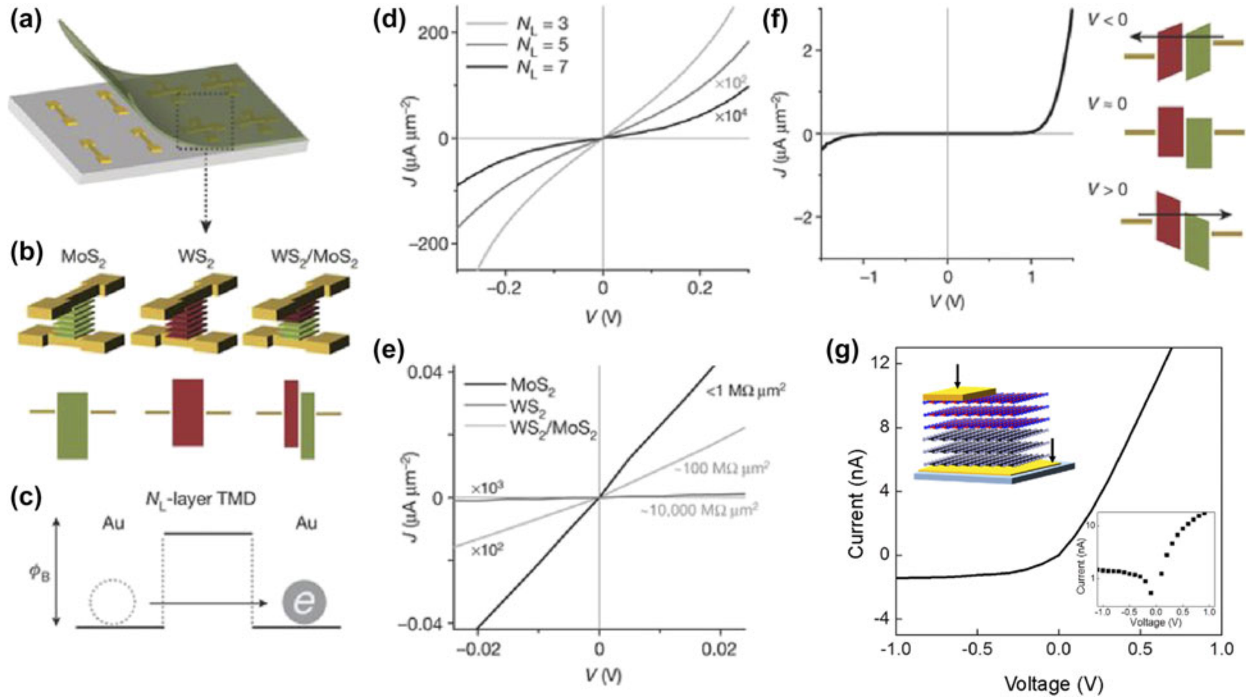

Figure 9: Electrical properties of wafer-scale 2D TMD heterolayers. (a) Schematic of wafer-scale vertically stacked 2D TMD heterolayer-based tunneling devices. (b) Cross-bar geometry of the devices where 2D layers are sandwiched in between Au electrodes. (c) General band alignment of the tunnel devices where ϕ_B is the barrier height. (d) *J*–*V* characteristics from three Au/N_L-layer MoS_2/Au devices (N_L = 3, 5, and 7). (e) Low voltage range *J*–*V* curves measured from MoS_2, WS_2, and WS_2/MoS_2 devices, all with N_L = 6. (f) *J*–*V* curve obtained from the WS_2/MoS_2 device in a large voltage range and the band diagrams corresponding to reverse bias ($V < 0$), zero-bias ($V \approx 0$) and large forward bias ($V > 0$). (g) *I*–*V* curve obtained from vertically stacked MoS_2/WS_2 heterolayers with Au top/bottom electrodes exhibiting current rectification. The inset shows the corresponding device geometry and the *I*–*V* curve in the log-scale. (a–f) Reprinted with permission from Ref. [58]. Copyright © 2017, Springer Nature. (g) Reprinted with permission from Ref. [41]. Copyright © 2017, American Chemical Society. (color online)

tunneling under the forward bias because of the lowering of the tunnel barrier as depicted in the diagrams. Islam et al. also demonstrated similar current rectification from vertically stacked MoS_2/WS_2 heterolayers, shown in Fig. 9(g). The 2D heterolayers were fabricated via the one-step metal film transformation growth method and were subsequently transferred onto a secondary substrate followed by Au electrode contacts. The inset in Fig. 9(g) illustrates the device geometry as well as the corresponding current (*I*)–voltage (*V*) curve in the log-scale [41].

Outlooks and challenges

The last decade has witnessed the inception and development of various 2D TMD heterolayers, which has significantly enriched the ever-expanding library of 2D materials by judiciously combining their existing components of tailored optical and electrical properties. Because of their intrinsically anisotropic vdW bonding nature, arbitrarily stacking individual 2D TMD layers can realize the atomically thin device circumventing the major limitation of crystallographic lattice match demanded in conventional thin film growth technologies. Therefore, 2D TMD heterolayers render unique structures inaccessible in any natural or man-made materials, offering unprecedented opportunities not only for the fundamental investigation of near atomic-scale 2D interlayer interactions but also for customized design of electronics and optoelectronics devices with unconventional functionalities. A substantial amount of effort has been driven to explore strategies to fabricate 2D TMD heterolayers on a large industrially compatible wafer-scale, including direct CVD growth, mechanically or chemically driven transfer and integration of 2D layers, and many others. Despite the impressive advancements enabled by these approaches thoroughly discussed in this review, several major challenges remain hindering that the achieved 2D TMD heterolayers satisfy their projected true technological potential. Below, we discuss these issues in both terms of CVD growth- and mechanical integration–based preparation methods.

In the first place, the scalable fabrication of 2D TMD heterolayers begins with the preparation of individual large-area 2D TMD layers with atomically well-defined structure and chemistries. The precise control and retention of highly uniform lateral dimension, vertical thickness, and layer numbers in individual 2D TMD building blocks are critically important, thus is demanded in their initial growth stages. Despite the devoted efforts to investigate the fundamentals of

Journal of Materials Research ■ Volume 35 ■ Issue 11 ■ Jun15, 2020 ■ www.mrs.org/jmr

the CVD process, mature procedures for producing wafer-scale 2D TMD layers with structural and chemical quality comparable to those of their mechanically exfoliated flake forms remain unestablished. Further explorations of 2D TMD growth mechanisms through diverse in situ experimental techniques and theoretical calculations will be beneficial to gain insights into understanding the interfacial interaction of individual 2D layers at near-atomic scales, providing technical guidance toward their optimum growth conditions.

Secondly, the assembly of individual 2D TMD layers enabled by both sequential growth and mechanical transfer/integration approaches involves two critical issues. While each preassembled or grown constituting 2D layer should retain structural integrity, the sequential stacking of secondary 2D layers either by chemical or physical means should preserve atomically flat and clean interfaces exposing well-defined 2D/2D interfacial vdW gaps to avoid unwanted scattering events for electron transports. The previously discussed two-step sequential CVD method is disadvantageous in terms of yielding an inevitable inter-diffusion of existing elements in between pre- and secondarily grown 2D layers, potentially leading to undesired material properties. While the one-step metal film transformation method intrinsically circumvents this problem, it is limited to grow 2D TMD layers sharing identical chalcogen elements only thus fails in achieving 2D TMD layers based on "arbitrary" components. Moreover, precise control of the 2D layer number over the entire growth wafer is still a major challenge common in both approaches. Physical approaches based on mechanical transfer and integration of separately prepared 2D TMD layers are intrinsically versatile as they can stack up arbitrary layers in a sequentially controlled order. However, most of these approaches rely on employing external chemicals to separate the initially prepared 2D TMD layers from their growth substrates, which often results in unavoidable residual chemicals at 2D layer interfaces [113]. Hence, innovative experimental designs that can comprehensively combine both these chemical and physical approaches accompanying atomic-level chemical precision and wafer-level structural scalability are imperative.

Last but not least, recent studies have verified that the controlled alignment and stacking of adjacent 2D layers achieving specifically targeted misorientation angles can make considerable impacts on their resulting electronic and optical properties [114, 115, 116]. Notwithstanding that the currently prevailing epitaxial chemical growth and manual stacking methods can produce 2D heterolayers of targeted orientation misorientation angles, the reproducible and precise control of sequentially stacked arbitrary 2D layers with programmable orientation alignment at wafer-scale is yet unavailable to date. It is anticipated that wafer-scale 2D heterolayers with encoded alignment profiles will bring forth a large set of exotic properties that have never been unveiled in conventional 2D heterostructures with random stacking alignments.

Despite the many challenges faced in their manufacturing aspects, the unusually superior material properties (e.g., high mechanical adaptability and exceptional heat dissipation) of 2D TMD heterolayers are extremely appealing that should not be overlooked in moving toward next-generation electronics and optoelectronics. With further advances of mass-production manufacturing strategies creatively enabling their desired stacking profiles, clean interfaces, and controlled orientations, the conceptually projected bright prospects of 2D TMD heterolayers are believed to be realized and significantly contributing to foster the revolution of emergent technologies.

Acknowledgments

This work was supported by the National Science Foundation (CMMI-1728390) (M.S.S., and Y.J.), the Korea Institute of Energy Technology Evaluation and Planning (KETEP), and the Ministry of Trade, Industry, and Energy (MOTIE) of the Republic of Korea (No. 20173010013340) (Y.J.). Y.J. also acknowledges VPR Advancement of Early Career Researchers award from the University of Central Florida. This research was in part supported by the Creative Materials Discovery Program through the National Research Foundation of Korea (NRF) funded by the Ministry of Science, ICT and Future Planning (NRF-2017M3D1A1039553).

References

1. **J.J. Gooding**: Nanostructuring electrodes with carbon nanotubes: A review on electrochemistry and applications for sensing. *Electrochim. Acta* **50**, 3049 (2005).
2. **Y. Li, F. Qian, J. Xiang, and C.M. Lieber**: Nanowire electronic and optoelectronic devices. *Mater. Today* **9**, 18 (2006).
3. **M. Trojanowicz**: Analytical applications of carbon nanotubes: A review. *TrAC, Trends Anal. Chem.* **25**, 480 (2006).
4. **M.J. Allen, V.C. Tung, and R.B. Kaner**: Honeycomb carbon: A review of graphene. *Chem. Rev.* **110**, 132 (2009).
5. **Y. Zhang, L. Zhang, and C. Zhou**: Review of chemical vapor deposition of graphene and related applications. *Acc. Chem. Res.* **46**, 2329 (2013).
6. **G.R. Bhimanapati, Z. Lin, V. Meunier, Y. Jung, J. Cha, S. Das, D. Xiao, Y. Son, M.S. Strano, and V.R. Cooper**: Recent advances in two-dimensional materials beyond graphene. *ACS Nano* **9**, 11509 (2015).
7. **C. Tan, X. Cao, X-J. Wu, Q. He, J. Yang, X. Zhang, J. Chen, W. Zhao, S. Han, and G-H. Nam**: Recent advances in ultrathin two-dimensional nanomaterials. *Chem. Rev.* **117**, 6225 (2017).
8. **H. Zhang**: Ultrathin two-dimensional nanomaterials. *ACS Nano* **9**, 9451 (2015).

9. **S. Das, J.A. Robinson, M. Dubey, H. Terrones, and M. Terrones**: Beyond graphene: Progress in novel two-dimensional materials and van der Waals solids. *Annu. Rev. Mater. Res.* **45**, 1 (2015).
10. **F. Wang, Z. Wang, Q. Wang, F. Wang, L. Yin, K. Xu, Y. Huang, and J. He**: Synthesis, properties and applications of 2D non-graphene materials. *Nanotechnology* **26**, 292001 (2015).
11. **K.F. Mak, C. Lee, J. Hone, J. Shan, and T.F. Heinz**: Atomically thin MoS_2: A new direct-gap semiconductor. *Phys. Rev. Lett.* **105**, 136805 (2010).
12. **H.J. Conley, B. Wang, J.I. Ziegler, R.F. Haglund, Jr., S.T. Pantelides, and K.I. Bolotin**: Bandgap engineering of strained monolayer and bilayer MoS_2. *Nano Lett.* **13**, 3626 (2013).
13. **S. Susarla, A. Kutana, J.A. Hachtel, V. Kochat, A. Apte, R. Vajtai, J.C. Idrobo, B.I. Yakobson, C.S. Tiwary, and P.M. Ajayan**: Quaternary 2D transition metal dichalcogenides (TMDs) with tunable bandgap. *Adv. Mater.* **29**, 1702457 (2017).
14. **X. Duan, C. Wang, Z. Fan, G. Hao, L. Kou, U. Halim, H. Li, X. Wu, Y. Wang, J. Jiang, A. Pan, Y. Huang, R. Yu, and X. Duan**: Synthesis of $WS_{2x}Se_{2-2x}$ alloy nanosheets with composition-tunable electronic properties. *Nano Lett.* **16**, 264 (2016).
15. **X. Bao, Q. Ou, Z-Q. Xu, Y. Zhang, Q. Bao, and H. Zhang**: Band structure engineering in 2D materials for optoelectronic applications. *Adv. Mater. Technol.* **3**, 1800072 (2018).
16. **H. Sahin, S. Tongay, S. Horzum, W. Fan, J. Zhou, J. Li, J. Wu, and F. Peeters**: Anomalous Raman spectra and thickness-dependent electronic properties of WSe_2. *Phys. Rev. B* **87**, 165409 (2013).
17. **L. Gao**: Flexible device applications of 2D semiconductors. *Small* **13**, 1603994 (2017).
18. **C. Gong, Y. Zhang, W. Chen, J. Chu, T. Lei, J. Pu, L. Dai, C. Wu, Y. Cheng, and T. Zhai**: Electronic and optoelectronic applications based on 2D novel anisotropic transition metal dichalcogenides. *Adv. Sci.* **4**, 1700231 (2017).
19. **W. Choi, N. Choudhary, G.H. Han, J. Park, D. Akinwande, and Y.H. Lee**: Recent development of two-dimensional transition metal dichalcogenides and their applications. *Mater. Today* **20**, 116 (2017).
20. **M.S. Shawkat, H-S. Chung, D. Dev, S. Das, T. Roy, and Y. Jung**: Two-dimensional/three-dimensional Schottky junction photovoltaic devices realized by the direct CVD growth of vdw 2D $PtSe_2$ layers on silicon. *ACS Appl. Mater. Interfaces* **11**, 27251 (2019).
21. **K. Novoselov, A. Mishchenko, A. Carvalho, and A.C. Neto**: 2D materials and van der Waals heterostructures. *Science* **353**, aac9439 (2016).
22. **A.K. Geim and I.V. Grigorieva**: Van der Waals heterostructures. *Nature* **499**, 419 (2013).
23. **Y. Liu, Y. Huang, and X. Duan**: Van der Waals integration before and beyond two-dimensional materials. *Nature* **567**, 323 (2019).
24. **Y. Li, Y. Wang, L. Huang, X. Wang, X. Li, H.X. Deng, Z. Wei, and J. Li**: Anti-ambipolar field-effect transistors based on few-layer 2D transition metal dichalcogenides. *ACS Appl. Mater. Interfaces* **8**, 15574 (2016).
25. **X. Duan, C. Wang, A. Pan, R. Yu, and X. Duan**: Two-dimensional transition metal dichalcogenides as atomically thin semiconductors: Opportunities and challenges. *Chem. Soc. Rev.* **44**, 8859 (2015).
26. **R. Cheng, D. Li, H. Zhou, C. Wang, A. Yin, S. Jiang, Y. Liu, Y. Chen, Y. Huang, and X. Duan**: Electroluminescence and photocurrent generation from atomically sharp WSe_2/MoS_2 heterojunction p–n diodes. *Nano Lett.* **14**, 5590 (2014).
27. **J. Mann, Q. Ma, P.M. Odenthal, M. Isarraraz, D. Le, E. Preciado, D. Barroso, K. Yamaguchi, G. von Son Palacio, A. Nguyen, T. Tran, M. Wurch, A. Nguyen, V. Klee, S. Bobek, D. Sun, T.F. Heinz, T.S. Rahman, R. Kawakami, and L. Bartels**: 2-Dimensional transition metal dichalcogenides with tunable direct band gaps: $MoS_{2(1-x)}Se_{2x}$ monolayers. *Adv. Mater.* **26**, 1399 (2014).
28. **H. Li, X. Duan, X. Wu, X. Zhuang, H. Zhou, Q. Zhang, X. Zhu, W. Hu, P. Ren, and P. Guo**: Growth of alloy $MoS_{2X}Se_{2(1-X)}$ nanosheets with fully tunable chemical compositions and optical properties. *J. Am. Chem. Soc.* **136**, 3756 (2014).
29. **M.M. Furchi, A. Pospischil, F. Libisch, J. Burgdörfer, and T. Mueller**: Photovoltaic effect in an electrically tunable van der Waals heterojunction. *Nano Lett.* **14**, 4785 (2014).
30. **Y. Gong, J. Lin, X. Wang, G. Shi, S. Lei, Z. Lin, X. Zou, G. Ye, R. Vajtai, B.I. Yakobson, H. Terrones, M. Terrones, K. Beng Tay, J. Lou, S.T. Pantelides, Z. Liu, W. Zhou, and P.M. Ajayan**: Vertical and in-plane heterostructures from WS_2/MoS_2 monolayers. *Nat. Mater.* **13**, 1135 (2014).
31. **M.H. Naik and M. Jain**: Ultraflatbands and shear solitons in moire patterns of twisted bilayer transition metal dichalcogenides. *Phys. Rev. Lett.* **121**, 266401 (2018).
32. **F. Wu, T. Lovorn, E. Tutuc, and A.H. MacDonald**: Hubbard model physics in transition metal dichalcogenide moiré bands. *Phys. Rev. Lett.* **121**, 026402 (2018).
33. **H. Heo, J.H. Sung, S. Cha, B-G. Jang, J-Y. Kim, G. Jin, D. Lee, J-H. Ahn, M-J. Lee, and J.H. Shim**: Interlayer orientation-dependent light absorption and emission in monolayer semiconductor stacks. *Nat. Commun.* **6**, 7372 (2015).
34. **B.V. Lotsch**: Vertical 2D heterostructures. *Annu. Rev. Mater. Res.* **45**, 85 (2015).
35. **Z. Cai, B. Liu, X. Zou, and H-M. Cheng**: Chemical vapor deposition growth and applications of two-dimensional materials and their heterostructures. *Chem. Rev.* **118**, 6091 (2018).
36. **N. Choudhary, J. Park, J.Y. Hwang, H-S. Chung, K.H. Dumas, S.I. Khondaker, W. Choi, and Y. Jung**: Centimeter scale patterned growth of vertically stacked few layer only 2D MoS_2/WS_2 van der Waals heterostructure. *Sci. Rep.* **6**, 25456 (2016).

37. **J.M. Woods, Y. Jung, Y. Xie, W. Liu, Y. Liu, H. Wang, and J.J. Cha**: One-step synthesis of MoS_2/WS_2 layered heterostructures and catalytic activity of defective transition metal dichalcogenide films. *ACS Nano* **10**, 2004 (2016).
38. **S.S. Han, J.H. Kim, C. Noh, J.H. Kim, E. Ji, J. Kwon, S.M. Yu, T-J. Ko, E. Okogbue, and K.H. Oh**: Horizontal-to-vertical transition of 2D layer orientation in low-temperature chemical vapor deposition-grown $PtSe_2$ and its influences on electrical properties and device applications. *ACS Appl. Mater. Interfaces* **11**, 13598 (2019).
39. **D. Kong, H. Wang, J.J. Cha, M. Pasta, K.J. Koski, J. Yao, and Y. Cui**: Synthesis of MoS_2 and $MoSe_2$ films with vertically aligned layers. *Nano Lett.* **13**, 1341 (2013).
40. **Y. Jung, J. Shen, Y. Liu, J.M. Woods, Y. Sun, and J.J. Cha**: Metal seed layer thickness-induced transition from vertical to horizontal growth of MoS_2 and WS_2. *Nano Lett.* **14**, 6842 (2014).
41. **M.A. Islam, J.H. Kim, A. Schropp, H. Kalita, N. Choudhary, D. Weitzman, S.I. Khondaker, K.H. Oh, T. Roy, H.S. Chung, and Y. Jung**: Centimeter-scale 2D van der Waals vertical heterostructures integrated on deformable substrates enabled by gold sacrificial layer-assisted growth. *Nano Lett.* **17**, 6157 (2017).
42. **Y. Jung, J. Shen, Y. Sun, and J.J. Cha**: Chemically synthesized heterostructures of two-dimensional molybdenum/tungsten-based dichalcogenides with vertically aligned layers. *ACS Nano* **8**, 9550 (2014).
43. **D. Chiappe, I. Asselberghs, S. Sutar, S. Iacovo, V. Afanas'ev, A. Stesmans, Y. Balaji, L. Peters, M. Heyne, and M. Mannarino**: Controlled sulfurization process for the synthesis of large area MoS_2 films and MoS_2/WS_2 heterostructures. *Adv. Mater. Interfaces* **3**, 1500635 (2016).
44. **C.R. Wu, X.R. Chang, T.W. Chu, H.A. Chen, C.H. Wu, and S.Y. Lin**: Establishment of 2D crystal heterostructures by sulfurization of sequential transition metal depositions: Preparation, characterization, and selective growth. *Nano Lett.* **16**, 7093 (2016).
45. **H. Liu, S.L. Wong, and D. Chi**: CVD growth of MoS_2-based two-dimensional materials. *Chem. Vap. Deposition* **21**, 241 (2015).
46. **X. Duan, C. Wang, J.C. Shaw, R. Cheng, Y. Chen, H. Li, X. Wu, Y. Tang, Q. Zhang, and A. Pan**: Lateral epitaxial growth of two-dimensional layered semiconductor heterojunctions. *Nat. Nanotechnol.* **9**, 1024 (2014).
47. **Z. Zhang, P. Chen, X. Duan, K. Zang, J. Luo, and X. Duan**: Robust epitaxial growth of two-dimensional heterostructures, multiheterostructures, and superlattices. *Science* **357**, 788 (2017).
48. **Z. Lin, A. McCreary, N. Briggs, S. Subramanian, K. Zhang, Y. Sun, X. Li, N.J. Borys, H. Yuan, and S.K. Fullerton-Shirey**: 2D materials advances: From large scale synthesis and controlled heterostructures to improved characterization techniques, defects and applications. *2D Mater.* **3**, 042001 (2016).
49. **S. Xie, L. Tu, Y. Han, L. Huang, K. Kang, K.U. Lao, P. Poddar, C. Park, D.A. Muller, and R.A. DiStasio**: Coherent, atomically thin transition-metal dichalcogenide superlattices with engineered strain. *Science* **359**, 1131 (2018).
50. **K. Kang, S. Xie, L. Huang, Y. Han, P.Y. Huang, K.F. Mak, C-J. Kim, D. Muller, and J. Park**: High-mobility three-atom-thick semiconducting films with wafer-scale homogeneity. *Nature* **520**, 656 (2015).
51. **S. Vishwanath, X. Liu, S. Rouvimov, L. Basile, N. Lu, A. Azcatl, K. Magno, R.M. Wallace, M. Kim, and J-C. Idrobo**: Controllable growth of layered selenide and telluride heterostructures and superlattices using molecular beam epitaxy. *J. Mater. Res.* **31**, 900 (2016).
52. **H.C. Diaz, Y. Ma, R. Chaghi, and M. Batzill**: High density of (pseudo) periodic twin-grain boundaries in molecular beam epitaxy-grown van der Waals heterostructure: $MoTe_2/MoS_2$. *Appl. Phys. Lett.* **108**, 191606 (2016).
53. **C. Zhang, Y. Chen, J-K. Huang, X. Wu, L-J. Li, W. Yao, J. Tersoff, and C-K. Shih**: Visualizing band offsets and edge states in bilayer–monolayer transition metal dichalcogenides lateral heterojunction. *Nat. Commun.* **7**, 10349 (2016).
54. **Y-C. Lin, R.K. Ghosh, R. Addou, N. Lu, S.M. Eichfeld, H. Zhu, M-Y. Li, X. Peng, M.J. Kim, and L-J. Li**: Atomically thin resonant tunnel diodes built from synthetic van der Waals heterostructures. *Nat. Commun.* **6**, 7311 (2015).
55. **S. Vishwanath, X. Liu, S. Rouvimov, P.C. Mende, A. Azcatl, S. McDonnell, R.M. Wallace, R.M. Feenstra, J.K. Furdyna, and D. Jena**: Comprehensive structural and optical characterization of MBE grown $MoSe_2$ on graphite, CaF_2 and graphene. *2D Mater.* **2**, 024007 (2015).
56. **W. Mortelmans, S. El Kazzi, A.N. Mehta, D. Vanhaeren, T. Conard, J. Meersschaut, T. Nuytten, S. De Gendt, M. Heyns, and C. Merckling**: Peculiar alignment and strain of 2D WSe_2 grown by van der Waals epitaxy on reconstructed sapphire surfaces. *Nanotechnology* **30**, 465601 (2019).
57. **Y. Dai, X. Ren, J. Zhang, J. Liu, H. Liu, W. Ho, X. Dai, C. Jin, and M. Xie**: Multifarious interfaces, band alignments, and formation asymmetry of WSe_2–$MoSe_2$ heterojunction grown by molecular-beam epitaxy. *ACS Appl. Mater. Interfaces* **11**, 43766 (2019).
58. **K. Kang, K-H. Lee, Y. Han, H. Gao, S. Xie, D.A. Muller, and J. Park**: Layer-by-Layer assembly of two-dimensional materials into wafer-scale heterostructures. *Nature* **550**, 229 (2017).
59. **Z. Yan, T. Pan, M. Xue, C. Chen, Y. Cui, G. Yao, L. Huang, F. Liao, W. Jing, and H. Zhang**: Thermal release transfer printing for stretchable conformal bioelectronics. *Adv. Sci.* **4**, 1700251 (2017).
60. **K. Liu, L. Zhang, T. Cao, C. Jin, D. Qiu, Q. Zhou, A. Zettl, P. Yang, S.G. Louie, and F. Wang**: Evolution of interlayer coupling in twisted molybdenum disulfide bilayers. *Nat. Commun.* **5**, 4966 (2014).

61. **A.V. Kretinin, Y. Cao, J.S. Tu, G.L. Yu, R. Jalil, K.S. Novoselov, S.J. Haigh, A. Gholinia, A. Mishchenko, M. Lozada, T. Georgiou, C.R. Woods, F. Withers, P. Blake, G. Eda, A. Wirsig, C. Hucho, K. Watanabe, T. Taniguchi, A.K. Geim, and R.V. Gorbachev**: Electronic properties of graphene encapsulated with different two-dimensional atomic crystals. *Nano Lett.* **14**, 3270 (2014).

62. **M-H. Chiu, M-Y. Li, W. Zhang, W-T. Hsu, W-H. Chang, M. Terrones, H. Terrones, and L-J. Li**: Spectroscopic signatures for interlayer coupling in MoS_2–WSe_2 van der Waals stacking. *ACS Nano* **8**, 9649 (2014).

63. **B. Huang, G. Clark, E. Navarro-Moratalla, D.R. Klein, R. Cheng, K.L. Seyler, D. Zhong, E. Schmidgall, M.A. McGuire, D.H. Cobden, W. Yao, D. Xiao, P. Jarillo-Herrero, and X. Xu**: Layer-dependent ferromagnetism in a van der Waals crystal down to the monolayer limit. *Nature* **546**, 270 (2017).

64. **J. Shim, S.H. Bae, W. Kong, D. Lee, K. Qiao, D. Nezich, Y.J. Park, R. Zhao, S. Sundaram, X. Li, H. Yeon, C. Choi, H. Kum, R. Yue, G. Zhou, Y. Ou, K. Lee, J. Moodera, X. Zhao, J.H. Ahn, C. Hinkle, A. Ougazzaden, and J. Kim**: Controlled crack propagation for atomic precision handling of wafer-scale two-dimensional materials. *Science* **362**, 665 (2018).

65. **H. Li, J.K. Huang, Y. Shi, and L.J. Li**: Toward the growth of high mobility 2D transition metal dichalcogenide semiconductors. *Adv. Mater. Interfaces* **6**, 1900220 (2019).

66. **K.S. Novoselov, A.K. Geim, S.V. Morozov, D. Jiang, Y. Zhang, S.V. Dubonos, I.V. Grigorieva, and A.A. Firsov**: Electric field effect in atomically thin carbon films. *Science* **306**, 666 (2004).

67. **S.B. Desai, S.R. Madhvapathy, M. Amani, D. Kiriya, M. Hettick, M. Tosun, Y. Zhou, M. Dubey, J.W. Ager, III, D. Chrzan, and A. Javey**: Gold-mediated exfoliation of ultralarge optoelectronically-perfect monolayers. *Adv. Mater.* **28**, 4053 (2016).

68. **D. Rhodes, S.H. Chae, R. Ribeiro-Palau, and J. Hone**: Disorder in van der Waals heterostructures of 2D materials. *Nat. Mater.* **18**, 541 (2019).

69. **Z. Xu and M.J. Buehler**: Interface structure and mechanics between graphene and metal substrates: A first-principles study. *J. Phys.: Condens. Matter* **22**, 485301 (2010).

70. **T. Björkman, A. Gulans, A.V. Krasheninnikov, and R.M. Nieminen**: Van der Waals bonding in layered compounds from advanced density-functional first-principles calculations. *Phys. Rev. Lett.* **108**, 235502 (2012).

71. **Z. Suo and J.W. Hutchinson**: Steady-state cracking in brittle substrates beneath adherent films. *Int. J. Solids Struct.* **25**, 1337 (1989).

72. **J.H. Kim, T.J. Ko, E. Okogbue, S.S. Han, M.S. Shawkat, M.G. Kaium, K.H. Oh, H.S. Chung, and Y. Jung**: Centimeter-scale green integration of layer-by-layer 2D tmd vdw heterostructures on arbitrary substrates by water-assisted layer transfer. *Sci. Rep.* **9**, 1641 (2019).

73. **Y.C. Lin, W. Zhang, J.K. Huang, K.K. Liu, Y.H. Lee, C.T. Liang, C.W. Chu, and L.J. Li**: Wafer-scale MoS_2 thin layers prepared by MoO_3 sulfurization. *Nanoscale* **4**, 6637 (2012).

74. **K.K. Liu, W. Zhang, Y.H. Lee, Y.C. Lin, M.T. Chang, C.Y. Su, C.S. Chang, H. Li, Y. Shi, H. Zhang, C.S. Lai, and L.J. Li**: Growth of large-area and highly crystalline MoS_2 thin layers on insulating substrates. *Nano Lett.* **12**, 1538 (2012).

75. **A. Gurarslan, Y. Yu, L. Su, Y. Yu, F. Suarez, S. Yao, Y. Zhu, M. Ozturk, Y. Zhang, and L. Cao**: Surface-energy-assisted perfect transfer of centimeter-scale monolayer and few-layer MoS_2 films onto arbitrary substrates. *ACS Nano* **8**, 11522 (2014).

76. **H. Li, T-J. Ko, M. Lee, H-S. Chung, S.S. Han, K.H. Oh, A. Sadmani, H. Kang, and Y. Jung**: Experimental realization of few layer two-dimensional MoS_2 membranes of near atomic thickness for high efficiency water desalination. *Nano Lett.* **19**, 5194 (2019).

77. **M.A. Islam, J.H. Kim, T-J. Ko, C. Noh, S. Nehate, M.G. Kaium, M. Ko, D. Fox, L. Zhai, and C-H. Cho**: Three dimensionally-ordered 2D MoS_2 vertical layers integrated on flexible substrates with stretch-tunable functionality and improved sensing capability. *Nanoscale* **10**, 17525 (2018).

78. **E. Okogbue, J.H. Kim, T-J. Ko, H-S. Chung, A. Krishnaprasad, J.C. Flores, S. Nehate, M.G. Kaium, J.B. Park, and S-J. Lee**: Centimeter-scale periodically corrugated few-layer 2D MoS_2 with tensile stretch-driven tunable multifunctionalities. *ACS Appl. Mater. Interfaces* **10**, 30623 (2018).

79. **N. Choudhary, H.S. Chung, J.H. Kim, C. Noh, M.A. Islam, K.H. Oh, K. Coffey, Y. Jung, and Y. Jung**: Strain-driven and layer-number-dependent crossover of growth mode in van der Waals heterostructures: 2D/2D layer-by-layer horizontal epitaxy to 2D/3D vertical reorientation. *Adv. Mater. Interfaces* **5**, 1800382 (2018).

80. **M.A. Islam, J. Church, C. Han, H-S. Chung, E. Ji, J.H. Kim, N. Choudhary, G-H. Lee, W.H. Lee, and Y. Jung**: Noble metal-coated MoS_2 nanofilms with vertically-aligned 2D layers for visible light-driven photocatalytic degradation of emerging water contaminants. *Sci. Rep.* **7**, 14944 (2017).

81. **E. Okogbue, S.S. Han, T-J. Ko, H-S. Chung, J. Ma, M.S. Shawkat, J.H. Kim, E. Ji, K. Oh, and L. Zhai**: Multifunctional two-dimensional $PtSe_2$-layer kirigami conductors with 2000% stretchability and metallic-to-semiconducting tunability. *Nano Lett.* **19**, 7598 (2019).

82. **T. Suni, K. Henttinen, I. Suni, and J. Mäkinen**: Effects of plasma activation on hydrophilic bonding of Si and SiO_2. *J. Electrochem. Soc.* **149**, G348 (2002).

83. **H. Wang, B. Yu, S. Jiang, L. Jiang, and L. Qian**: UV/ozone-assisted tribochemistry-induced nanofabrication on Si(100). *Surfaces RSC advances.* **7**, 39651 (2017).

84. **A. Alam, M. Howlader, and M. Deen**: The effects of oxygen plasma and humidity on surface roughness, water contact angle

and hardness of silicon, silicon dioxide and glass. *J. Micromech. Microeng.* **24**, 035010 (2014).

85. **J. Lee, P. Dak, Y. Lee, H. Park, W. Choi, M.A. Alam, and S. Kim**: Two-dimensional layered MoS_2 biosensors enable highly sensitive detection of biomolecules. *Sci. Rep.* **4**, 7352 (2014).
86. **C.R. Wu, X.R. Chang, C.H. Wu, and S.Y. Lin**: The growth mechanism of transition metal dichalcogenides by using sulfurization of pre-deposited transition metals and the 2D crystal hetero-structure establishment. *Sci. Rep.* **7**, 42146 (2017).
87. **Y. Xue, Y. Zhang, Y. Liu, H. Liu, J. Song, J. Sophia, J. Liu, Z. Xu, Q. Xu, Z. Wang, J. Zheng, Y. Liu, S. Li, and Q. Bao**: Scalable production of a few-layer MoS_2/WS_2 vertical heterojunction array and its application for photodetectors. *ACS Nano* **10**, 573 (2016).
88. **Y. Gong, S. Lei, G. Ye, B. Li, Y. He, K. Keyshar, X. Zhang, Q. Wang, J. Lou, Z. Liu, R. Vajtai, W. Zhou, and P.M. Ajayan**: Two-step growth of two-dimensional $WSe_2/MoSe_2$ heterostructures. *Nano Lett.* **15**, 6135 (2015).
89. **H. Liu, S. Hussain, A. Ali, B.A. Naqvi, D. Vikraman, W. Jeong, W. Song, K-S. An, and J. Jung**: A vertical WSe_2–$MoSe_2$ P–N heterostructure with tunable gate rectification. *RSC Adv.* **8**, 25514 (2018).
90. **M. Mahjouri-Samani, M.W. Lin, K. Wang, A.R. Lupini, J. Lee, L. Basile, A. Boulesbaa, C.M. Rouleau, A.A. Puretzky, I.N. Ivanov, K. Xiao, M. Yoon, and D.B. Geohegan**: Patterned arrays of lateral heterojunctions within monolayer two-dimensional semiconductors. *Nat. Commun.* **6**, 7749 (2015).
91. **R. Ghosh, J-S. Kim, A. Roy, H. Chou, M. Vu, S.K. Banerjee, and D. Akinwande**: Large area chemical vapor deposition growth of monolayer $MoSe_2$ and its controlled sulfurization to MoS_2. *J. Mater. Res.* **31**, 917 (2016).
92. **P.J. Zomer, S.P. Dash, N. Tombros, and B.J. Van Wees**: A transfer technique for high mobility graphene devices on commercially available hexagonal boron nitride. *Appl. Phys. Lett.* **99**, 232104 (2011).
93. **C-H. Lee, G-H. Lee, A.M. Van Der Zande, W. Chen, Y. Li, M. Han, X. Cui, G. Arefe, C. Nuckolls, T.F. Heinz, J. Guo, J. Hone, and P. Kim**: Atomically thin P–N junctions with van der Waals heterointerfaces. *Nat. Nanotechnol.* **9**, 676 (2014).
94. **G. Michael, G. Hu, D. Zheng, and Y. Zhang**: Piezo-phototronic solar cell based on 2D monochalcogenides materials. *J. Phys. D: Appl. Phys.* **52**, 204001 (2019).
95. **Y-H. Lee, L. Yu, H. Wang, W. Fang, X. Ling, Y. Shi, C-T. Lin, J-K. Huang, M-T. Chang, C-S. Chang, M. Dresselhaus, T. Palacios, L-J. Li, and J. Kong**: Synthesis and transfer of single-layer transition metal disulfides on diverse surfaces. *Nano Lett.* **13**, 1852 (2013).
96. **A. Castellanos-Gomez, M. Buscema, R. Molenaar, V. Singh, L. Janssen, H.S.J. Van Der Zant, and G.A. Steele**: Deterministic transfer of two-dimensional materials by all-dry viscoelastic stamping. *2D Mater.* **1**, 011002 (2014).
97. **H. Li, J. Wu, X. Huang, Z. Yin, J. Liu, and H. Zhang**: A universal, rapid method for clean transfer of nanostructures onto various substrates. *ACS Nano* **8**, 6563 (2014).
98. **A. Reina, X. Jia, J. Ho, D. Nezich, H. Son, V. Bulovic, M.S. Dresselhaus, and J. Kong**: Large area, few-layer graphene films on arbitrary substrates by chemical vapor deposition. *Nano Lett.* **9**, 30 (2009).
99. **C.R. Dean, A.F. Young, I. Meric, C. Lee, L. Wang, S. Sorgenfrei, K. Watanabe, T. Taniguchi, P. Kim, and K.L. Shepard**: Boron nitride substrates for high-quality graphene electronics. *Nat. Nanotechnol.* **5**, 722 (2010).
100. **S. Bertolazzi, J. Brivio, and A. Kis**: Stretching and breaking of ultrathin MoS_2. *ACS Nano* **5**, 9703 (2011).
101. **D.H. Tien, J-Y. Park, K.B. Kim, N. Lee, and Y. Seo**: Characterization of graphene-based fet fabricated using a shadow mask. *Sci. Rep.* **6**, 25050 (2016).
102. **T. Uwanno, Y. Hattori, T. Taniguchi, K. Watanabe, and K. Nagashio**: Fully dry pmma transfer of graphene on h-BN using a heating/cooling system. *2D Mater.* **2**, 041002 (2015).
103. **F. Bonaccorso, A. Lombardo, T. Hasan, Z. Sun, L. Colombo, and A.C. Ferrari**: Production and processing of graphene and 2D crystals. *Mater. Today* **15**, 564 (2012).
104. **X. Wang, K. Kang, S. Chen, R. Du, and E-H. Yang**: Location-specific growth and transfer of arrayed MoS_2 monolayers with controllable size. *2D Mater.* **4**, 025093 (2017).
105. **B. Hunt, J. Sanchez-Yamagishi, A. Young, M. Yankowitz, B.J. LeRoy, K. Watanabe, T. Taniguchi, P. Moon, M. Koshino, and P. Jarillo-Herrero**: Massive Dirac fermions and hofstadter butterfly in a van der Waals heterostructure. *Science* **340**, 1427 (2013).
106. **J.Y. Hong, Y.C. Shin, A. Zubair, Y. Mao, T. Palacios, M.S. Dresselhaus, S.H. Kim, and J. Kong**: A rational strategy for graphene transfer on substrates with rough features. *Adv. Mater.* **28**, 2382 (2016).
107. **X. Li, Y. Zhu, W. Cai, M. Borysiak, B. Han, D. Chen, R.D. Piner, L. Colombo, and R.S. Ruoff**: Transfer of large-area graphene films for high-performance transparent conductive electrodes. *Nano Lett.* **9**, 4359 (2009).
108. **S. Boandoh, F.O-T. Agyapong-Fordjour, S.H. Choi, J.S. Lee, J-H. Park, H. Ko, G. Han, S.J. Yun, S. Park, Y-M. Kim, W. Yang, Y.H. Lee, S.M. Kim, and K.K. Kim**: Wafer-scale van der Waals heterostructures with ultraclean interfaces via the aid of viscoelastic polymer. *ACS Appl. Mater. Interfaces* **11**, 1579 (2019).
109. **G-H. Lee, X. Cui, Y.D. Kim, G. Arefe, X. Zhang, C-H. Lee, F. Ye, K. Watanabe, T. Taniguchi, P. Kim, and J. Hone**: Highly stable, dual-gated MoS_2 transistors encapsulated by hexagonal boron nitride with gate-controllable contact, resistance, and threshold voltage. *ACS Nano* **9**, 7019 (2015).
110. **M. Choi, Y.J. Park, B.K. Sharma, S-R. Bae, S.Y. Kim, and J-H. Ahn**: Flexible active-matrix organic light-emitting diode

display enabled by MoS_2 thin-film transistor. *Sci. Adv.* **4**, eaas8721 (2018).

111. **M.Y. Chan, K. Komatsu, S-L. Li, Y. Xu, P. Darmawan, H. Kuramochi, S. Nakaharai, A. Aparecido-Ferreira, K. Watanabe, and T. Taniguchi**: Suppression of thermally activated carrier transport in atomically thin MoS_2 on crystalline hexagonal boron nitride substrates. *Nanoscale* **5**, 9572 (2013).
112. **V.V. Afanas'ev**: Electron band alignment at interfaces of semiconductors with insulating oxides: An internal photoemission study. *Adv. Condens. Matter Phys.* **2014**, 1 (2014).
113. **D.G. Purdie, N.M. Pugno, T. Taniguchi, K. Watanabe, A.C. Ferrari, and A. Lombardo**: Cleaning interfaces in layered materials heterostructures. *Nat. Commun.* **9**, 5387 (2018).
114. **Y. Cao, V. Fatemi, S. Fang, K. Watanabe, T. Taniguchi, E. Kaxiras, and P. Jarillo-Herrero**: Unconventional superconductivity in magic-angle graphene superlattices. *Nature* **556**, 43 (2018).
115. **Y. Cao, V. Fatemi, A. Demir, S. Fang, S.L. Tomarken, J.Y. Luo, J.D. Sanchez-Yamagishi, K. Watanabe, T. Taniguchi, E. Kaxiras, R.C. Ashoori, and P. Jarillo-Herrero**: Correlated insulator behaviour at half-filling in magic-angle graphene superlattices. *Nature* **556**, 80 (2018).
116. **Y. Cao, J. Luo, V. Fatemi, S. Fang, J. Sanchez-Yamagishi, K. Watanabe, T. Taniguchi, E. Kaxiras, and P. Jarillo-Herrero**: Superlattice-induced insulating states and valley-protected orbits in twisted bilayer graphene. *Phys. Rev. Lett.* **117**, 116804 (2016).